J Membrane Biol (2011) 239:137–156
DOI 10.1007/s00232-010-9333-7

Gating-Related Molecular Motions in the Extracellular Domain of the I_{Ks} Channel: Implications for I_{Ks} Channelopathy

Yu Hong Wang · Min Jiang · Xu Lin Xu · Kai-Ling Hsu · Mei Zhang · Gea-Ny Tseng

Received: 9 September 2010 / Accepted: 15 November 2010 / Published online: 9 December 2010

Abstract Cardiac slow delayed rectifier (I_{Ks}) channel complex consists of KCNQ1 channel and KCNE1 auxiliary subunits. The extracellular juxtamembranous region of KCNE1 is an unstructured loop that contacts multiple KCNQ1 positions in a gating-state-dependent manner. Congenital arrhythmia-related mutations have been identified in the extracellular S1–S2 linker of KCNQ1. These mutations manifest abnormal phenotypes only when coexpressed with KCNE1, pointing to the importance of proper KCNQ1/KCNE1 interactions here in I_{Ks} channel function. We investigate the interactions between the KCNE1 loop (positions 36–47) and KCNQ1 S1–S2 linker (positions 140–148) by means of disulfide trapping and voltage clamp techniques. During transitions among the resting-state conformations, KCNE1 positions 36–43 make contacts with KCNQ1 positions 144, 145, and 147 in a parallel fashion. During conformational changes in the activated state, KCNE1 position 40 can make contacts with all three KCNQ1 positions, while the neighboring KCNE1 positions (36, 38, 39, and 41) can make contact with KCNQ1 position 147. Furthermore, KCNQ1 positions 143 and 146 are high-impact positions that cannot tolerate cysteine substitution. To maintain the proper I_{Ks} channel function, position 143 requires a small side chain with a hydroxyl group, and position 146 requires a negatively charged side chain. These data and the proposed molecular motions provide insights into the mechanisms by which mutations in the extracellular juxtamembranous region of the I_{Ks} channel impair its function.

Keywords Voltage-gated K channels · Structure–function relationship · Voltage clamp

The slow delayed rectifier (I_{Ks}) channel functions as a repolarization reserve in the human heart (Jost et al. 2005). Its importance in maintaining the cardiac electrical stability is indicated by I_{Ks} channelopathy; that is, mutations in its molecular components can cause congenital arrhythmia (long QT syndrome types 1 and 5, LQT1 and LQT5, and short QT syndrome type 2/familial atrial fibrillation, SQT2/fAF) (Chen et al. 2003b; Hong et al. 2005; Kapplinger et al. 2009; Splawski et al. 2000). The I_{Ks} channel has two major components: a pore-forming KCNQ1 channel (also known as Kv7.1 or KvLQT1, abbreviated as Q1) and auxiliary KCNE1 subunits (also known as mink or IsK, abbreviated as E1) (Sanguinetti et al. 1996). Q1 is a typical voltage-gated potassium (Kv) channel formed by four subunits surrounding a central pore. Each subunit has six transmembrane segments (S1–S6) and a pore-lining (P) loop between S5 and S6. In a Q1 channel, S1–S4 of the four subunits form four peripheral voltage-sensing domains, and the four copies of S5-P-loop-S6 together form the central pore domain (PD) (Fig. 1a, b). E1 is a type I single-membrane-spanning protein (Fig. 1b). Although multiple KCNE subunits are expressed in the human heart (Bendahhou et al. 2005; Lundquist et al. 2005; Radicke et al. 2006) and each of them can associate with the Q1 channel to confer distinct channel phenotypes (Bendahhou et al. 2005; Grunnet et al. 2005), E1 is an obligate component of the I_{Ks} channel. This

Electronic supplementary material The online version of this article (doi:10.1007/s00232-010-9333-7) contains supplementary material, which is available to authorized users.

Y. H. Wang · M. Jiang · X. L. Xu · K.-L. Hsu · M. Zhang · G.-N. Tseng (✉)
Department of Physiology and Biophysics, Virginia Commonwealth University, 1101 E. Marshall Street, Sanger 3-042a, Richmond, VA 23298, USA
e-mail: gtseng@vcu.edu

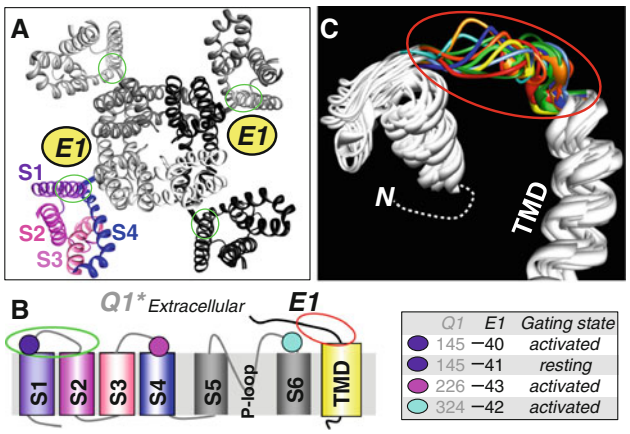

Fig. 1 Region of interest in the (KCN)Q1/(KCN)E1 (I_{Ks}) channel complex. **a** Cartoon of a Q1/E1 channel complex viewed from the extracellular side of the cell membrane. The Q1 channel is simulated by the Kv1.2 crystal structure (2A79.pdb; Long et al. 2005). Three of the Q1 subunits are shown as *light–dark gray ribbons*. The fourth (*lower left*) subunit has S1, S2, S3, and S4 color coded (*purple, magenta, pink, and blue*) and labeled. Region of interest in Q1 (extracellular S1–S2 linker) is highlighted by *open green ovals*. Two E1 subunits are associated with one Q1 channel (Chen et al. 2003a; Morin and Kobertz 2008), and their TMDs (*yellow circles*) are assumed to occupy diagonal spaces between voltage-sensing domains of two adjacent Q1 subunits. **b** *Left* Two-dimensional diagram of Q1/E1 transmembrane helices, marking region of interest in Q1 (*green oval*), region of interest in E1 (*red oval*), and Q1 positions where engineered Cys side chains can form disulfide bonds with Cys engineered into E1. *Right* List of Q1 and E1 positions that can be disulfide bonded when both are occupied by Cys residues, and the gating state (activated or resting) conformation that allows disulfide formation (Chung et al. 2009; Nakajo and Kubo 2007; Xu et al. 2008). **c** Ten nuclear magnetic resonance structures of E1 (2K21.pdb, Kang et al. 2008) are superimposed as *white ribbons*, except the region of interest (color-coded for individual structures and enclosed by a *red open oval*). The TMD and relative position of the N-terminus are marked

is because only E1 can confer the distinct I_{Ks} phenotype upon the Q1 channel: a positive voltage range of activation coinciding with the plateau phase of cardiac action potential, and uniquely slow rates of activation and deactivation.

There has been a long-standing interest in understanding the structure–function relationship of the I_{Ks} channel. Experimental data support a major stoichiometry of E1:Q1 of 2:4 (two E1 subunits per Q1 tetramer channel) (Chen et al. 2003a; Morin and Kobertz 2008; however, see Nakajo et al. 2010). Furthermore, the transmembrane domain (TMD) of E1 may reside in the space (cleft) between voltage-sensing domains of two adjacent Q1 subunits, juxtaposed to the pore domain of the Q1 channel (Fig. 1a, assuming that the 2 E1 TMDs occupy the diagonal clefts in the Q1 channel). E1 makes extensive contacts with Q1, including the transmembrane region (Melman et al. 2001; Panaghie et al. 2006; Tai and Goldstein 1998; Tapper and George 2001), the cytoplasmic region (Haitin et al. 2009; Lvov et al. 2010; Wiener et al. 2008), and the extracellular region (Chung et al. 2009; Nakajo and Kubo 2007; Xu et al. 2008). Q1/E1 interactions in the transmembrane region determine the I_{Ks} pore conductance (Sesti and Goldstein 1998; Yang and Sigworth 1998) and gating kinetics (Melman et al. 2001), while Q1/E1 interactions in the cytoplasmic region influence I_{Ks} trafficking (Ghosh et al. 2006; Shamgar et al. 2006), modulation by protein kinase A-mediated phosphorylation (Kurokawa et al. 2009), and gating kinetics (Lvov et al. 2010; Wu et al. 2006). However, the functional roles of Q1/E1 interactions in the extracellular region are not clear.

Figure 1 illustrates the region in the I_{Ks} channel examined in this study (region of interest): the extracellular juxtamembranous region of E1 (highlighted by the open red ovals in panels B and C), and the S1–S2 linker of Q1 (highlighted by the open green ovals in panels A and B). Previous work using cysteine (Cys) substitution mutagenesis and disulfide trapping experiments has shown that several positions on Q1 come close to E1 positions 40–43 to allow disulfide bond formation (Chung et al. 2009; Nakajo and Kubo 2007; Xu et al. 2008). Interestingly, these Q1 positions are scattered at the extracellular ends of S1, S4 and S6, and disulfide formation with E1 occurs in a gating-state dependent manner (Fig. 1b). These observations suggest that the E1 structure around positions 40–43 must be very flexible, that can engage in conformational changes during I_{Ks} gating transitions and allow contacts with multiple sites on the Q1 channel. Indeed, the E1 nuclear magnetic resonance structures show that the extracellular juxtamembranous region of E1 is an unstructured loop (Fig. 1c) (Kang et al. 2008), potentially capable of swinging and turning.

We are particularly interested in the interactions between this extracellular E1 loop and the S1–S2 linker of Q1. Recent studies suggest that the S1 is not merely a structural element and a passive bystander during Kv channel gating transitions. Instead, S1 is an active participant in the gating processes. For example, in the Shaker channel, the extracellular end of S1 comes close to the S4 in the closed state, participating in the formation of a hydrophobic seal that creates a highly focused transmembrane electrical field around the first arginine on S4 (Campos et al. 2007). In the KvAP channel, the S1 occupies a central location in the voltage-sensing domain and interacts with the pore domain (Cuello et al. 2004). The S1–S2 linker of the Q1 channel harbors a high density of congenital arrhythmia-related mutations: S140G (Chen et al. 2003b), V141M (Hong et al. 2005), S143L (Liu et al. 2006), T144A (Zareba et al. 2003), E146K (Napolitano et al. 2005), and Q147R (Lundby et al. 2007). Importantly, three of these mutations (S140G, V141M, and Q147R) manifest their abnormal phenotypes only when coexpressed with E1. Therefore, Q1/E1

interactions in the extracellular region of the I_{Ks} channel are critical for its function, but the underlying mechanisms are not clear.

We start out by addressing two main questions: (1) What is the pattern of contacts between the extracellular juxtamembranous region of E1 (positions 36–47) and the S1–S2 linker of Q1 (positions 140–148)? (2) What is the relationship between these Q1/E1 contacts and the I_{Ks} channel gating function? We use disulfide trapping experiments (nonreducing immunoblots of whole cell lysates from COS-7 cells) and voltage clamp experiments (in oocytes) to address these questions. Pilot experiments show that although Cys substitution is well tolerated at 7 of the 9 Q1 positions, for the remaining 2 positions, 143 and 146, Cys substitution impairs Q1 protein folding and trafficking. Therefore, these 2 Q1 positions are excluded from the disulfide trapping and voltage clamp experiments. Instead, we make a series of mutations at these 2 positions to address a third question: (3) to maintain proper Q1 channel function, what are the requirements for side chain properties at positions 143 and 146? Our data and interpretation are discussed in the context of I_{Ks} channelopathy.

Methods

Voltage clamp experiments reported here are conducted on oocytes from frogs (*Xenopus laevis*). The animal protocol is reviewed and approved annually by Institutional Animal Care and Use Committee of Virginia Commonwealth University.

Molecular Biology and Side-directed Mutagenesis

Human Q1 and E1 cDNAs are generous gifts from Dr. MT Keating (Harvard University) and R Sansom (Merck Company), respectively. We use a short isoform 0 (581 aa) of Q1 (Sanguinetti et al. 1996), that has a shorter cytoplasmic amino terminus than the long isoform 1 (676 aa) but exhibits the same gating properties and the same pattern of modulation by KCNE subunits (Liu et al. 2007). For comparison with the literature, we use the same numbering of isoform 1 to specify Q1 positions where cysteine substitution is made. All the Cys-substituted Q1 constructs are made in a Cys-free background (Q1*-WT) that have all the native Cys residues replaced by Ala (Xu et al. 2008). Q1*-WT is similar to the parent Q1-WT in gating properties, ion selectivity and KCNE modulation (Xu et al. 2008). The Q1 constructs are in vector pcDNA3.1/V5-His-TOPO (Invitrogen, for COS-7 expression) or pSP64 (Promega, for oocyte expression). In the former case, in-frame V5 and His_{6x} epitopes are attached to the carboxyl terminus of Q1, which do not perturb Q1 channel function or Q1/E1 interaction (Xu et al. 2008). E1 is subcloned into pAlter-Max (Promega, COS-7 and oocyte expression). Mutations are created using the QuickChange mutagenesis kit (Invitrogen), and confirmed by direct DNA sequencing. For in vitro transcription, plasmids are linearized by a suitable restriction enzyme, and transcribed using SP6 or T7 RNA polymerase and commercial kits (Mmessage Mmachine, Ambion, TX). The cRNA products are run on denaturing RNA gels and stained with ethidium bromide. The cRNA band sizes and intensities are quantified by densitometry (ChemiImager model 4400, Alpha-Innotech Corp), using a known amount of RNA size markers as reference.

COS-7 Expression and Western Blot Testing

COS-7 cells are maintained in D-MEM (Gibco) supplemented with 10% fetal calf serum (Hyclone) and penicillin/streptomycin, in a moist 5% CO_2 chamber at 36°C. Cells are transfected with Q1 and E1 cDNAs at a molar ratio of 1:1. Forty-eight hours after transfection, COS-7 cells are scraped off petri dishes and incubated in 20 mM N-ethylmaleimide (NEM) on ice for 10 min before making whole cell lysate. Cells are lysed by repeated freeze/thawing cycles in a lysis buffer (2% triton X-100, 10% glycerol, 62.5 mM Tris–HCl, 1 mM EDTA, pH 6.8). After low-speed centrifugation to remove nuclei and mitochondria, the whole cell lysates are treated with 2% sodium dodecyl sulfate (SDS) to disrupt noncovalent protein–protein associations. In some experiments, whole cell lysates are treated with dithiothreitol (DTT) (10 mM, 10 min, room temperature) to reduce disulfide bonds. Protein samples are loaded onto 4–20% gradient nonreducing SDS polyacrylamide gels. After fractionation, the proteins are blotted onto PVDF (polyvinylidene diflouride) membranes (Amersham), and probed for Q1 (V5 mAb from Invitrogen) or E1 pAb (Alomone). Immunoreactivity is visualized using an ECL detection kit (Amersham), and band intensities are quantified by densitometry (ChemiImager model 4400).

Cross-linking

Forty-eight hours after transfection, COS-7 cells are incubated with 10 mM DTT at room temperature. After thorough rinsing to remove DTT, cells are reacted with 2 mM of bifunctional thiol-reactive methanethiosulfonate cross-linkers containing 3 to 6 spacer arm carbon atoms (Toronto Research Chemicals) at 4°C for 15 min. The reaction is stopped by adding 10 mM NEM. The cells are subjected to whole cell lysis followed by SDS–polyacrylamide gel electrophoresis (PAGE), all under nonreducing conditions. After blotting the proteins to PVDF, the membrane is probed with V5 mAb for visualizing Q1 bands.

Oocyte Expression and Two-cushion Pipette Voltage Clamp Recording

Oocytes are isolated as described before (Tseng-Crank et al. 1990), and incubated in an ND96-based medium (in mM: NaCl 96, KCl 2, $CaCl_2$ 1.8, $MgCl_2$ 1, HEPES 5, Na-pyruvate 2.5, pH 7.5), supplemented with 4% horse serum and penicillin/streptomycin at 16°C. Two to 4 hr after isolation, oocytes are injected with cRNA or cRNAs using a Drummond digital microdispenser. Each oocyte receives 5 ng of Q1 cRNA alone or with 1.5 ng of E1 (molar ratio 1:1). Whole oocyte membrane currents are recorded using the two-cushion pipette voltage clamp method (Schreibmayer et al. 1994). Both current-passing and voltage-recording pipettes have a low tip resistance of 0.2–0.6 MΩ for good voltage clamp conditions. During recordings, the oocyte is continuously superfused with a low-Cl ND96 solution (Cl^- ions in ND96 replaced by methanesulfonate) to reduce interference from endogenous Cl channels. The bath solution is connected to the Ag-AgCl pellets in the grounding half-cells by salt bridges filled with 1% agarose in 3 M KCl. Voltage clamp is performed at room temperature (21–24°C) with OC-725C (Warner Instruments, MA) or GeneClamp 500 (Molecular Devices). Voltage clamp protocol generation and data acquisition are controlled by pClamp 10 via DigiData 1440A (Molecular Devices). Current data are low-pass filtered at 1 kHz (Frequency Devices, MA) and stored on disks for off-line analysis. The voltage clamp protocols and methods of data analysis are described in the figure captions and the table footnotes. The following software is used for data analysis: pClamp 10, Excel (Microsoft), SigmaPlot, SigmaStat, and PeakFit (SPSS).

Results

Pattern of Spontaneous Disulfide Formation Between Cys Side Chains Engineered into Regions of Interest in Q1 and E1

We are interested in identifying spontaneous disulfide formation between engineered Cys side chains. For two Cys side chains to form a disulfide bond, they need to come close to each other with a distance of $\leq$6 Å between the two C_β atoms (Careaga and Falke 1992) at least transiently during the protein's conformational changes. Thus, the pattern of spontaneous disulfide formation between Q1 and E1 can inform us on how the two parts of the I_{Ks} channel interact with each other. This information, in conjunction with the knowledge of *when* the disulfide bonds are formed, i.e. whether they are formed in the resting or activated state conformations, can be used as spatial restraints in building the I_{Ks} channel structure models in different gating states.

All our Cys-substituted Q1 constructs are made in a Cys-free background (Q1*-WT, with all native Cys residues replaced by Ala). There is one native Cys (C106) in the cytoplasmic domain of E1. In our experiments disulfide bonds are formed when the channels are still in the cell membrane. All free thiol groups are covalently modified by a cell membrane permeable thiol-modifying reagent NEM (20 mM) before the channels are solubilized from the cell membrane. Therefore, the cytoplasmic C106 is not likely to form a disulfide bond with Cys engineered into Q1's extracellular domain.

Figure 2a depicts current traces recorded from oocytes expressing Q1*-WT or Q1* with Cys engineered into the region of interest (positions 140–148, excluding 143 and 146, see below), alone or with E1-WT. The channels' gating parameters are listed in Table 1. All seven Cys-substituted Q1* mutants retain the key features of E1 modulation: slowing of activation, positive shift in the half-maximum activation voltage ($V_{0.5}$) and decrease in the equivalent gating charge (z_g). Figure 2b depicts current traces from oocytes expressing Q1*-WT, alone, with E1-WT, or with E1 having Cys substituted into positions 36–47. The related gating parameters are listed in Table 2. In all 12 cases, coexpressing Cys-substituted E1 mutants with Q1*-WT causes a slowing of activation, positive shift in $V_{0.5}$ and a decrease in z_g, similar to the effects of E1-WT. Therefore, these Cys-substituted Q1* and E1 mutants retain the key features of interactions between the two components of the I_{Ks} channel. This is critical since we want to use the information of disulfide bond formation between Cys-substituted Q1* and E1 to deduce their contacts in the native I_{Ks} channel. However, removing native Cys residues from Q1 causes a −30 mV shift in its $V_{0.5}$ of activation and may impact on the interactions between the voltage-sensing domain of Q1 and the extracellular loop of E1.

COS-7 cells are transfected with Cys-substituted Q1* and E1 pairs and cultured under standard conditions to allow spontaneous disulfide formation. Forty-eight hours after transfection, cells are incubated with NEM before membrane solubilization to prevent nonnative disulfide formation. All the following procedures are carried out under nonreducing conditions (unless otherwise specified) to preserve those spontaneously formed disulfide bonds. Whole cell lysates are made under strong denaturing conditions to disrupt noncovalently associated Q1* and E1, and the Q1* protein species are analyzed by SDS-PAGE followed by immunoblotting. Our previous experience has shown that Q1* monomer migrates as a 60 kDa band, and disulfide bonded Q1*/E1 heterodimer migrates as an 80 kDa band (sometimes with an additional faint 75 kDa band). Interestingly, disulfide bonded Q1*/E1 heterodimer

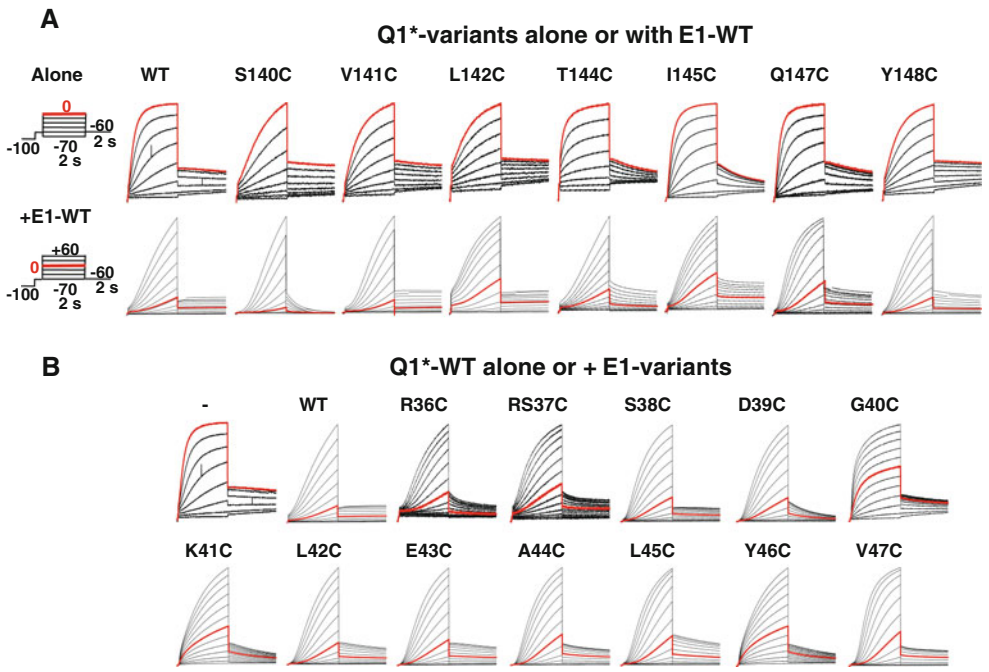

Fig. 2 Cys substitution at Q1* positions 140–148 (excluding 143 and 146) or E1 positions 36–47 does not perturb the Q1*/E1 interactions. **a** Representative current traces from oocytes expressing Q1*-WT or Cys-substituted mutants alone (*top row*), or coexpressed with E1-WT (*bottom row*). The voltage clamp protocols are diagrammed on the *left*. Current traces elicited by test pulses to 0 mV are shown in *red* to highlight the differences in the voltage dependence of activation when the Q1* variants are coexpressed with E1-WT. **b** Representative current traces from oocytes expressing Q1*-WT expressed alone (—, *upper left panel*), or coexpressed with E1-WT or Cys-substituted mutants. The voltage clamp protocols are the same as those diagrammed in **a**. *Red traces* highlight currents elicited by test pulses to 0 mV

cannot be recognized by E1 antibodies targeting the carboxyl terminus of E1 (Xu et al. 2008).

All our immunoblot experiments include the following controls to guard against false-negative conclusions: (a) Q1*-I145C/E1-G40C, that can form a strong disulfide bond (Xu et al. 2008), is included as a positive control to ensure the nonreducing conditions, and (b) the expression of all the Cys-substituted E1 constructs in the same set of COS-7 cells is confirmed to ensure the presence of disulfide bonding partners. To guard against false positive conclusions, we include a negative control in all our immunoblot experiments: Cys-substituted Q1* constructs expressed alone or with E1-WT (having only one engineered Cys, not allowing disulfide formation between Q1* and E1). For key Q1*/E1 pairs that form putative disulfide bonds, we also check whether DTT treatment of the whole cell lysates abolishes the 80 and 75 kDa bands.

Figure 3 illustrates representative immunoblot experiments probing disulfide formation between Cys engineered into Q1 position 144 (Q1*-T144C, Fig. 3a) or 147 (Q1*-Q147C, Fig. 3b) and Cys engineered into E1 positions 36–43. Under nonreducing conditions (top panels, labeled as "no DTT"), there is a distinct 80 kDa band (and for some, a fainter 75 kDa band) when Q1*-T144C is paired with E1-G40C or -K41C, and when Q1*-Q147C is paired with E1-R36C, -S37C, -S38C, -G40C or -K41C. When either Q1* construct is paired with E1-WT, only the 60 kDa Q1* monomer band is seen (left most lanes). Importantly, treating the whole cell lysates with DTT abolishes these distinct 80 and 75 kDa bands (middle panels, labeled as "with DTT"), confirming that they represent disulfide bonded Q1*/E1 heterodimers.

Much fainter 80 and 75 kDa bands are also seen with several other Cys-substituted Q1*/E1 pairs (top panels of Fig. 3a, b): Q1*-T144C paired with E1-R36C, and Q1*-Q147C paired with E1-D39C, -L42C or -E43C. The E1 immunoblots from the same set of COS-7 whole cell lysates confirm that all the E1 constructs are expressed (lower panels). Thus, differences in the degree of disulfide formation among the Q1*/E1 pairs cannot be attributed to variations in the expression of disulfide bonding partners.

We pair each of the 7 Cys-substituted Q1* variants (S140C to Y148C, excluding S143C and E146C) with each of the 12 Cys-substituted E1 variants (R36C to V47C) in COS-7 expression, and analyze the degree of disulfide formation using nonreducing immunoblot experiments as shown in Fig. 3. Figure 4 summarizes the results. The degree of disulfide formation is quantified by the ratio of 80 kDa band intensity (plus the 75 kDa band, if detectable) to the 60 kDa band intensity. In cases when no 80 kDa

Table 1 Effects of cysteine substitution in the S1–S2 linker of KCNQ1 on the channel function and KCNQ1–KCNE1 interactions

Q1* variant[a]	E1	$V_{0.5}$ (mV)[b]	z_g[b]	ΔG_o (kcal/mol)[c]	Cys substitution-related $\Delta\Delta G_o$ (kcal/mol)[d]	E1-WT-induced $\Delta\Delta G_o$ (kcal/mol)[e]	n[f]
WT	–	−50.5 ± 0.7	3.42 ± 0.10	−4.19 ± 0.16			49
WT	WT	−4.7 ± 2.7	1.82 ± 0.07	0.08 ± 0.07		4.26 ± 0.17	21
S140C	–	−19.8 ± 1.9	1.94 ± 0.09	−0.95 ± 0.11	3.24 ± 0.19		17
S140C	WT	36.3 ± 1.6	1.77 ± 0.09	1.52 ± 0.04		2.47 ± 0.12	10
V141C	–	−32.8 ± 2.5	1.86 ± 0.11	−1.54 ± 0.20	2.65 ± 0.26		17
V141C	WT	20.0 ± 3.0	1.52 ± 0.07	0.74 ± 0.14		2.28 ± 0.24	5
L142C	–	−39.1 ± 1.0	2.10 ± 0.09	−1.97 ± 0.10	2.21 ± 0.19		12
L142C	WT	12.3 ± 9.0	1.50 ± 0.16	0.35 ± 0.31		2.32 ± 0.33	4
T144C	–	−41.5 ± 1.9	2.05 ± 0.05	−2.03 ± 0.07	2.16 ± 0.18		6
T144C	WT	40.2 ± 3.1	1.10 ± 0.02	1.07 ± 0.09		3.10 ± 0.12	7
I145C	–	−45.8 ± 0.8	2.65 ± 0.08	−2.91 ± 0.12	1.27 ± 0.20		8
I145C	WT	15.4 ± 2.4	1.14 ± 0.02	0.41 ± 0.06		3.33 ± 0.13	7
Q147C	–	−49.2 ± 1.2	3.31 ± 0.11	−3.91 ± 0.14	0.28 ± 0.22		6
Q147C	WT	−0.1 ± 2.2	1.78 ± 0.06	−0.02 ± 0.10		3.89 ± 0.17	9
Y148C	–	−44.9 ± 1.1	2.50 ± 0.09	−2.71 ± 0.14	1.47 ± 0.22		11
Y148C	WT	17.9 ± 3.7	1.62 ± 0.11	0.62 ± 0.12		3.34 ± 0.18	9

[a] The Cys substitution mutations are made in a Cys-free background (Q1*-WT) in which all the native Cys residues have been replaced by Ala. Q1*-WT retains all key features of Q1 channel function in terms of activation gating, ion selectivity, and modulation by KCNE subunits, except a left shift in the activation curve along with a slowing of deactivation (Xu et al. 2008). The Q1* variants are expressed alone or with E1-WT in oocytes (5 and 1.5 ng of Q1* and E1 cRNA per oocyte, molar ratio 1:1). All oocytes are pretreated with DTT (10 mM, 10 min at room temperature) followed by thorough rinsing before recording

[b] Channels are activated by 2-s depolarizing pulses from a holding voltage of −100 or −110 mV to various test voltages (V_t) that cover the range of channel activation (between −90 and +10 mV in the case of Q1* variants expressed alone, and between −60 and up to +120 mV in the case of Q1* variants coexpressed with E1-WT). The peak amplitudes of tail currents (I_{tail}) are measured at −60 mV. The relationship between V_t and I_{tail} is fit with a Boltzmann function, $I_{tail} = I_{max}/(1 + \exp[(V_{0.5} - V_t)(RT/F)z_g])$, where I_{max}, $V_{0.5}$, and z_g are the estimated values of maximal I_{tail}, half-maximum activation voltage, and the number of apparent gating charges, respectively; and R, T, and F are the gas constant, temperature in °K, and the Faraday constant

[c] The apparent free energy of channel activation at 0 mV (ΔG_o) is calculated based on the 2-s isochronal activation curve described in (b), as $\Delta G_o = V_{0.5} * z_g * F$

[d] Cys-substitution-related change in the free energy of Q1* channel activation (when expressed alone) is calculated as $\Delta\Delta G_o = \Delta G_o^{Mut} - \Delta G_o^{WT}$, where ΔG_o^{Mut} and ΔG_o^{WT} are ΔG_o values for Cys-substituted Q1* mutant and Q1*-WT, respectively. The SE value for $\Delta\Delta G_o$ is calculated as the square root of sum of squares of SE values for ΔG_o^{Mut} and ΔG_o^{WT}

[e] E1-WT induced change in the free energy of channel activation ($\Delta\Delta G_o$) is calculated as $\Delta\Delta G_o = \Delta G_o^{QE} - \Delta G_o^{Q}$, where ΔG_o^{QE} and ΔG_o^{Q} are values of Q1* variant coexpressed with E1-WT and alone, respectively. The SE value for $\Delta\Delta G_o$ is calculated as the square root of sum of squares of SE values for ΔG_o^{QE} and ΔG_o^{Q}

[f] Number of oocytes studied

band is detectable, even after prolonged exposure of the films to the ECL reagents (so that the signals from the 60 kDa Q1* monomer bands are oversaturatetd), the data are denoted by (0) in Fig. 4. For most Q1*/E1 pairs, repetitive measurements are made and the number of measurements are listed adjacent to the histogram bars in Fig. 4. We define a ratio (80:60 kDa band intensities) of 0.1 as the threshold of significant disulfide formation. This ratio is denoted by the dotted lines in Fig. 4. Data points above this threshold are highlighted by black histogram bars. The relation between the Q1 positions examined and Q1's transmembrane S1 and S2 helices is indicated on the right margin of Fig. 4, while the relation between the E1 positions examined and the E1 transmembrane helix is indicated below the plots. The gradient in background shading is used to highlight the extracellular juxtamembranous region of the Q1*/E1 channel complex (light background) where multiple disulfide forming pairs are detected.

Relating the Pattern of Disulfide Bond Formation to the I_{Ks} Channel Function

The COS-7 immunoblot experiments can detect Q1* and E1 trapped in a disulfide-bonded state. However, they do not reveal the functional state or states of the Q1*/E1 channel

Table 2 Effects of cysteine substitution in the extracellular juxtamembranous loop of KCNE1 on the modulation of KCNQ1 channel function[a]

Q1* variant	E1 variant	$V_{0.5}$ (mV)	z_g	ΔG_o (kcal/mol)	E1-variant-induced $\Delta\Delta G_o$ (kcal/mol)	*n*
WT	–	−50.5 ± 0.7	3.42 ± 0.10	−4.19 ± 0.16		49
WT	WT	−4.7 ± 2.7	1.82 ± 0.07	0.08 ± 0.07	4.26 ± 0.17	21
WT	R36C	1.7 ± 7.8	1.76 ± 0.12	−0.13 ± 0.38	4.06 ± 0.41	11
WT	S37C	4.5 ± 4.2	1.56 ± 0.05	0.12 ± 0.16	4.31 ± 0.22	13
WT	S38C	−1.4 ± 4.1	1.56 ± 0.07	−0.08 ± 0.16	4.11 ± 0.22	11
WT	D39C	4.3 ± 4.8	1.67 ± 0.10	0.02 ± 0.20	4.21 ± 0.26	18
WT	G40C	−7.4 ± 6.4	1.65 ± 0.15	−0.66 ± 0.32	3.53 ± 0.35	18
WT	K41C	−20.7 ± 1.8	2.06 ± 0.09	−1.14 ± 0.13	3.05 ± 0.21	34
WT	L42C	3.8 ± 3.2	1.73 ± 0.04	0.12 ± 0.14	4.31 ± 0.21	26
WT	E43C	4.4 ± 2.7	1.73 ± 0.05	0.13 ± 0.13	4.32 ± 0.20	26
WT	A44C	−4.6 ± 2.2	2.02 ± 0.08	−0.31 ± 0.11	3.88 ± 0.20	35
WT	L45C	−2.6 ± 2.6	1.88 ± 0.07	−0.20 ± 0.11	3.99 ± 0.20	34
WT	Y46C	−7.7 ± 2.3	1.26 ± 0.07	0.32 ± 0.10	3.86 ± 0.19	37
WT	V47C	−4.7 ± 3.9	2.15 ± 0.10	−0.37 ± 0.19	3.82 ± 0.25	16

[a] Oocytes are injected with cRNAs for Q1*-WT and E1 variant (5 and 1.5 ng, Q1*:E1 cRNA molar ratio 1:1). All oocytes are pretreated with DTT (10 mM, 10 min at room temperature) before recording. The voltage clamp protocol and data analysis are the same as those described for Table 1. E1 variant induced change in the free energy of channel activation ($\Delta\Delta G_o$) is the difference between ΔG_o value of Q1*-WT coexpressed with E1-WT or Cys-substituted E1 variant and ΔG_o value of Q1*-WT expressed alone

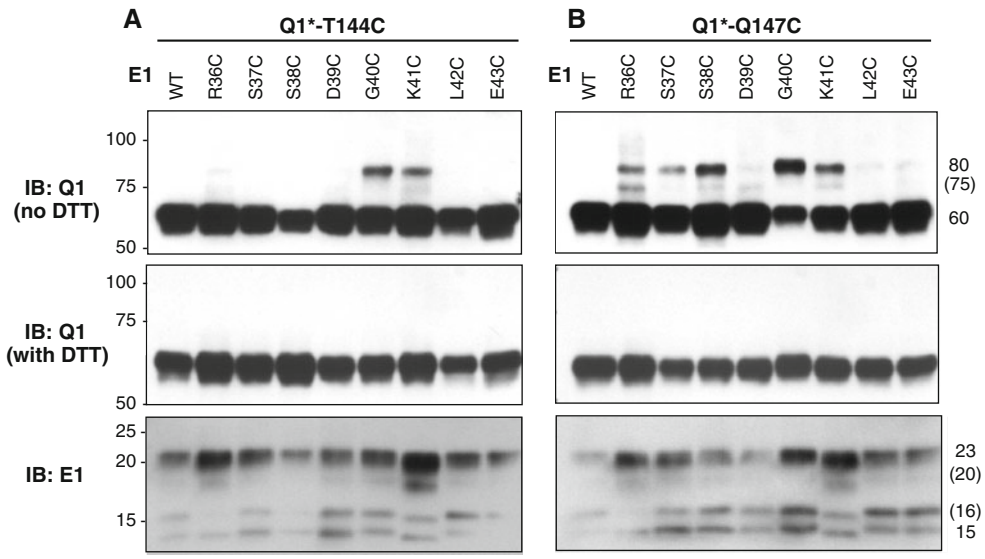

Fig. 3 Examples of using immunoblotting to detect disulfide bond formation between Q1* and E1. Cys is engineered into Q1* positions 144 (**a**) or 147 (**b**), in the Cys-removed Q1 background. The Q1* variants are coexpressed with Cys-substituted E1 mutants (positions 36–43, *marked on top*) and with E1-WT (*left most lanes*, serving as a negative control) in COS-7 cells at a cDNA molar ratio of 1:1. Cells are incubated with N-ethylmaleimide to protect all free thiol groups before being subjected to cell lysis under nonreducing conditions. Each sample of whole cell lysates is divided into two aliquots, one treated with DTT (10 mM, 10 min, room temperature) and other without. Samples are fractionated by nonreducing SDS-PAGE and probed for Q1 (*top and middle,* with V5 mAb targeting the V5 epitope appended to the Q1 carboxyl terminus) or E1 (*bottom*). The size marker bands are labeled on the *left*, and the target protein bands are marked on the *right*. Q1 monomer migrates as a 60-kDa band. Q1 disulfide bonded with E1 migrates principally as an 80 kDa band, but occasionally also as an additional faint 75-kDa band. E1 (with 2N-glycosylation sites, N6 and N26) migrated as unglycosylated (15 kDa) and differentially glycosylated (16, 20 and 23 kDa) bands

complex in which the disulfide bonds are formed. We study this issue by voltage clamp experiments in oocytes. Previously we have characterized the state-dependence of disulfide formation between Q1*-I145C and E1-G40C or -K41C (Xu et al. 2008). In this study, we focus on Q1*-Q147C and Q1*-T144C.

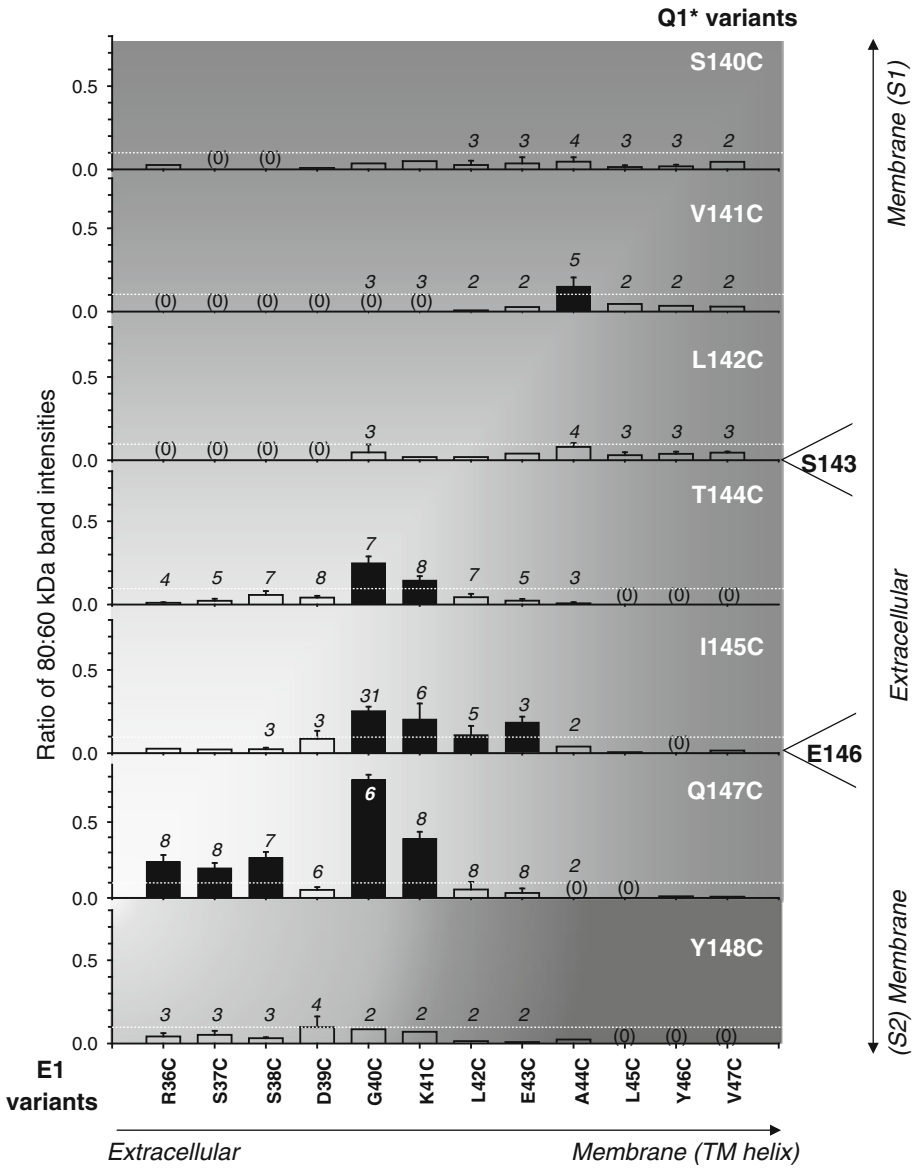

Fig. 4 Pattern of disulfide bond formation between Cys side chains engineered into Q1* positions 140 to 148 (excluding 143 and 146) and E1 positions 36–47. The degree of disulfide formation is quantified by the ratio of band intensity of disulfide-bonded Q1*/E1 (80 kDa, plus 75 kDa if detected) to that of Q1* monomer (60 kDa). Each panel plots the ratio of 80:60 kDa band intensities (coordinate), with the Q1* construct specified at the *upper right corner*, against the E1 variants listed along the abscissa. (0) denotes no detectable 80 kDa band. When experiments are repeated multiple times, the numbers of independent tests are noted adjacent to the *histogram bars*. The *white dotted lines* denote an 80:60 ratio of 0.1, defined as the threshold for significant disulfide bond formation between Q1* and E1. Data above the threshold are highlighted by *black histogram bars*

We choose to use the oocyte expression system for the functional tests for the following reasons. First, unlike the biochemical experiments in COS-7 cells where proteins from a population of cells are analyzed, voltage clamp experiments in individual cells require that the channel phenotypes (in our case, determined mainly by the ratio of Q1*:E1) be as uniform as possible. Oocyte expression allows us to precisely control the Q1*:E1 expression ratio by controlling the quantities of cRNAs injected. The integrity and concentrations of cRNA solutions of all the Q1* and E1 variants reported here are repetitively checked using denaturing RNA gels, and for the same expression experiment the cRNAs are often quantified on a single RNA gel for the best accuracy. The cRNA solutions are properly diluted/mixed before injection, so that each oocyte will receive the desired amounts of Q1* and E1 cRNAs (5 and 1.5 ng, respectively, molar ratio 1:1) when injected with 40 nl of the cRNA mix. To test whether the oocyte endogenous Q1 channel interferes with our data interpretation, in a subset of experiments we inject oocytes with E1-WT cRNA alone. Under the same voltage clamp conditions, these oocytes exhibit very little time-dependent outward currents that amount to $\leq$5% of the current amplitudes seen in oocytes coinjected with Q1* and E1 cRNAs (2-s test pulses to +60 mV). Second, in our previous study of Q1*-I145C paired with Cys-substituted E1 variants, the degree, and for Q1*-I145C/E1-G40C the state-dependence, of disulfide formation are well correlated between the COS-7 and oocyte expression systems (Xu et al. 2008). Third, oocytes provide robust and stable currents that allow us to study the effects of prolonged DTT exposure and washout (critical for our experiments

described below), unlike mammalian cells that cannot sustain DTT exposure (Lvov et al. 2010).

Previously, we determined the state-dependence of disulfide formation by testing whether spontaneous disulfide reformation (after reduction by DTT) required membrane depolarization to activate the channels (Fan et al. 1999; Xu et al. 2008). In the present study, there is little or no spontaneous disulfide reformation in most of the Q1*-Q147C or Q1*-T144C/Cys-substituted E1 pairs monitored for 10–20 min after DTT washout. Therefore, we use two alternative approaches to deducing the state-dependence of proximity between two engineered Cys side chains. The first approach is to test how reducing the spontaneously formed disulfide bonds by DTT affects the voltage dependence of channel activation. The second approach is to test the state-dependence of high-affinity Cd-bridge formation (see below).

If disulfide bonds are formed when the channels are in the resting state conformations, then disulfide bonding will stabilize the channels in the resting states, and stronger depolarization is needed to move the channel into the activated states and open. DTT reduces the disulfide bonds and destabilizes the resting states. This will shift the activation curve in the negative direction. On the other hand, if disulfide bonds are formed in the activated state conformations, it will stabilize the channels in the activated states, so that a relatively weak depolarization can activate the channels. Reducing the disulfide bonds by DTT will then shift the activation curve in the positive direction. This inference is supported by our published data (Xu et al. 2008), and validated by the state-dependence of Cd-bridge formation (see below). To summarize, a negative shift in $V_{0.5}$ by DTT is interpreted as disulfide bond formation in the resting states, while a positive shift in $V_{0.5}$ by DTT would suggest disulfide bond formation in the activated states.

State-dependence of Disulfide Formation When Q1*-Q147C is Paired with Cys-substituted E1 Variants

Figure 5a and b depicts two cases of DTT-induced shifts of activation curves. The complete data set is summarized in Fig. 5c. DTT exposure (10 mM, for 10–15 min) causes a small (<5 mV) negative shift of activation curves for Q1*-Q147C expressed alone or paired with E1-WT. This small $V_{0.5}$ shift is not different from those see in time control experiments (data not shown). However, DTT exposure induces a clear-cut positive shift of $V_{0.5}$ when Q1*-Q147C is paired with E1-R36C, -S38C, -D39C, -G40C, or -K41C. These observations suggest that disulfide bonds have been formed between Q1*-Q147C and these Cys-substituted E1 variants, and stabilize the channels in activated states. DTT reduces these disulfide bonds, destabilizing the activated states and shifting the activation curve in the positive direction. DTT exposure induces a prominent negative shift of $V_{0.5}$ when Q1*-Q147C is paired with E1-L42C or -E43C, that far exceeds the negative shifts seen with Q1*-Q147C expressed alone or paired with E1-WT. This suggests that disulfide bonds between Q1*-Q147C and E1-L42C or -E43C are formed in the resting states. Other than Q1*-Q147C/E1-G40C (and Q1*-Q147C/E1-S37C, discussed below), for the other Q1*-Q147C/E1 pairs the DTT-induced $V_{0.5}$ shifts are not reversed after washing out DTT for 10–20 min, indicating no disulfide reformation within this time.

We also monitor the rates of development of DTT effects on the Q1*-Q147C/Cys-substituted E1 pairs. Although the rate of DTT reduction can be influenced by DTT accessibility to the disulfide bond, in our study the region of interest is in the extracellular domain of the Q1/E1 channel complex, where the positions examined are exposed to the extracellular compartment and freely accessible to DTT. On the other hand, we envision that in the presence of DTT there are constant cycles of breaking and reformation of disulfide bonds between these engineered Cys side chains as the Q1 and E1 positions make contacts with each other during gating transitions. Therefore, the rate of development of DTT effects will be influenced by 2 factors: the chance of encounter between Cys side chains and the chemistry of the thiol groups. The first factor can be further broken down into 2 factors: the proximity between positions and the dynamic of peptide backbones bearing the Cys side chains. Our experiments do not evaluate contributions from these different factors quantitatively, and we lump them together in a qualitative term "strength of disulfide bond." Stronger disulfide bonds will be reduced by DTT at a slower rate than weak disulfide bonds. These data can be compared with the biochemical quantification of degrees of disulfide formation in COS-7 experiments shown in Fig. 4.

Figure 6 depicts representative time courses of development of DTT effects on Q1*-Q147C paired with Cys-substituted E1 variants, with Q1*-Q147C expressed alone or paired with E1-WT serving as negative controls. In most cases, the DTT effects are monitored with currents elicited by test pulses to voltages corresponding to the pre-DTT $V_{0.5}$ values ($V_{0.5}$ before DTT application). This is a sensitive indicator of DTT effects: current amplitude increases as $V_{0.5}$ is shifted in the negative direction (Fig. 5a), and decreases as $V_{0.5}$ is shifted in the positive direction (Fig. 5b). In cases where a prominent constitutive current component is seen (e.g. Q1*-Q147C paired with E1-R36C, -S38C or -K41C, Fig. 6, indicating that disulfide stabilizing the channels in activated states; Xu et al. 2008), the development of DTT effects is monitored by the rates of decrease in such constitutive component. Figure 6 shows that the time courses of development of DTT effects on the

Q1*-Q147C/Cys-substituted E1 pairs (other than Q1*-Q147C/E1-S37C, discussed below) can be well described by a single exponential function. The time constants of disulfide reduction by DTT are summarized in Fig. 7. The uniquely slow rate of disulfide reduction seen in Q1*-Q147C/E1-G40C, and its ability to reform the disulfide bond after DTT removal (Figs. 5c, 6), are consistent with the highest degree of disulfide formation in this Q1*/E1 pair observed in COS-7 experiments (Fig. 4).

Exposing Q1*-Q147C/E1-S37C to DTT causes a rapid (τ = 1–2 min) increase in the current amplitude monitored at the pre-DTT $V_{0.5}$ value, in conjunction with a negative shift in the activation curve (Fig. 5c). These observations suggest that disulfide bond between Q1*-Q147C and E1-S37C is formed in the resting state. However, the increase in current amplitude is followed by a gradual decline in the continuous presence of DTT (Fig. 6), so that when DTT is washed out, the $V_{0.5}$ value returns to the control value (Fig. 5c). The reason for the second phase of DTT effect is not clear.

Our data suggest that the side chain at Q1 position 147 can make contacts with 8 consecutive positions in the extracellular juxtamembranous E1 loop (positions 36–43). Five of the contacts occur in the activated states, and three occur in the resting states. Along this E1 loop, position 40 makes the most frequent or intimate contact with Q1 position 147, producing the highest degree and strongest disulfide bond among the Q1*/E1 pairs examined in both biochemical experiments (COS-7 cells) and voltage clamp experiments (oocytes).

State-dependence of Disulfide Formation When Q1*-T144C is Paired with Cys-substituted E1 Variants

Surprisingly, Q1*-T144C expressed alone or paired with E1-WT manifests a strong response to DTT (Fig. 8): in the presence of DTT the current amplitudes gradually decline and, in the case of Q1*-T144C/E1-WT, the activation curve is shifted in the positive direction (Supplementary Fig. S1A). Washing out DTT for 10–15 min produces little

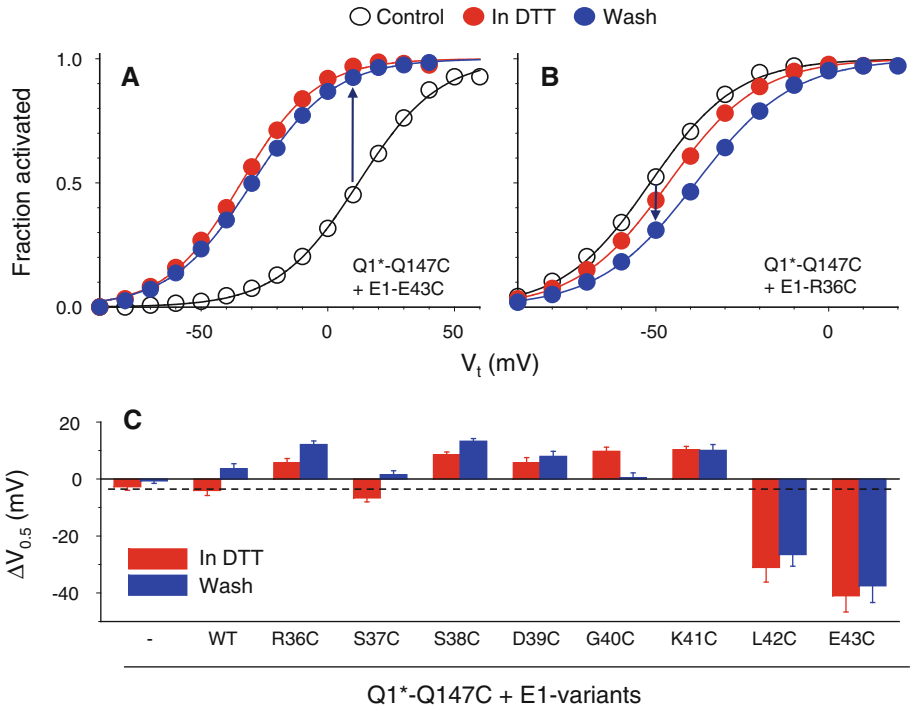

Fig. 5 Effects of DTT on the voltage dependence of activation of Q1*-Q147C expressed alone or with E1 variants. **a**, **b** Two examples of DTT-induced shift in the activation curve. Channel types are marked in the *insets*. Voltage clamp protocols are the same as those diagrammed in Fig. 2a. Tail current amplitudes (I_{tail}) at −60 mV are measured. The relationship between I_{tail} and test pulse voltage (V_t) is fit with a Boltzmann function $I_{tail} = I_{max}/(1 + \exp[(V_{0.5} - V_t)\ (RT/F)z_g])$, where I_{max}, $V_{0.5}$, and z_g are the estimated values of maximal I_{tail}, half-maximum activation voltage and the number of apparent gating charges, respectively, R, T, and F are the gas constant, temperature in K, and the Faraday constant. I_{tail} values are normalized by I_{max} as an estimate of fraction activated (coordinates). Measurements are made before, during (10–15 min after beginning DTT 10 mM application) and after (after washout for 10–15 min) DTT treatment. *Arrows* indicate the magnitudes and directions of changes in the current amplitude elicited by test pulses to $\sim V_{0.5}$ of activation under the control conditions, monitored during DTT wash-in and wash-out (Fig. 6). **c** Summary of shift in $V_{0.5}$ of activation ($\Delta V_{0.5}$) in the presence of DTT and after DTT washout for Q1*-Q147C expressed alone (—) or coexpressed with E1 variants. To facilitate comparison between Q1*-Q147C paired with Cys-substituted E1 variants vs. Q1*-Q147C/E1-WT, a *dotted line* is drawn across the latter data point obtained in DTT

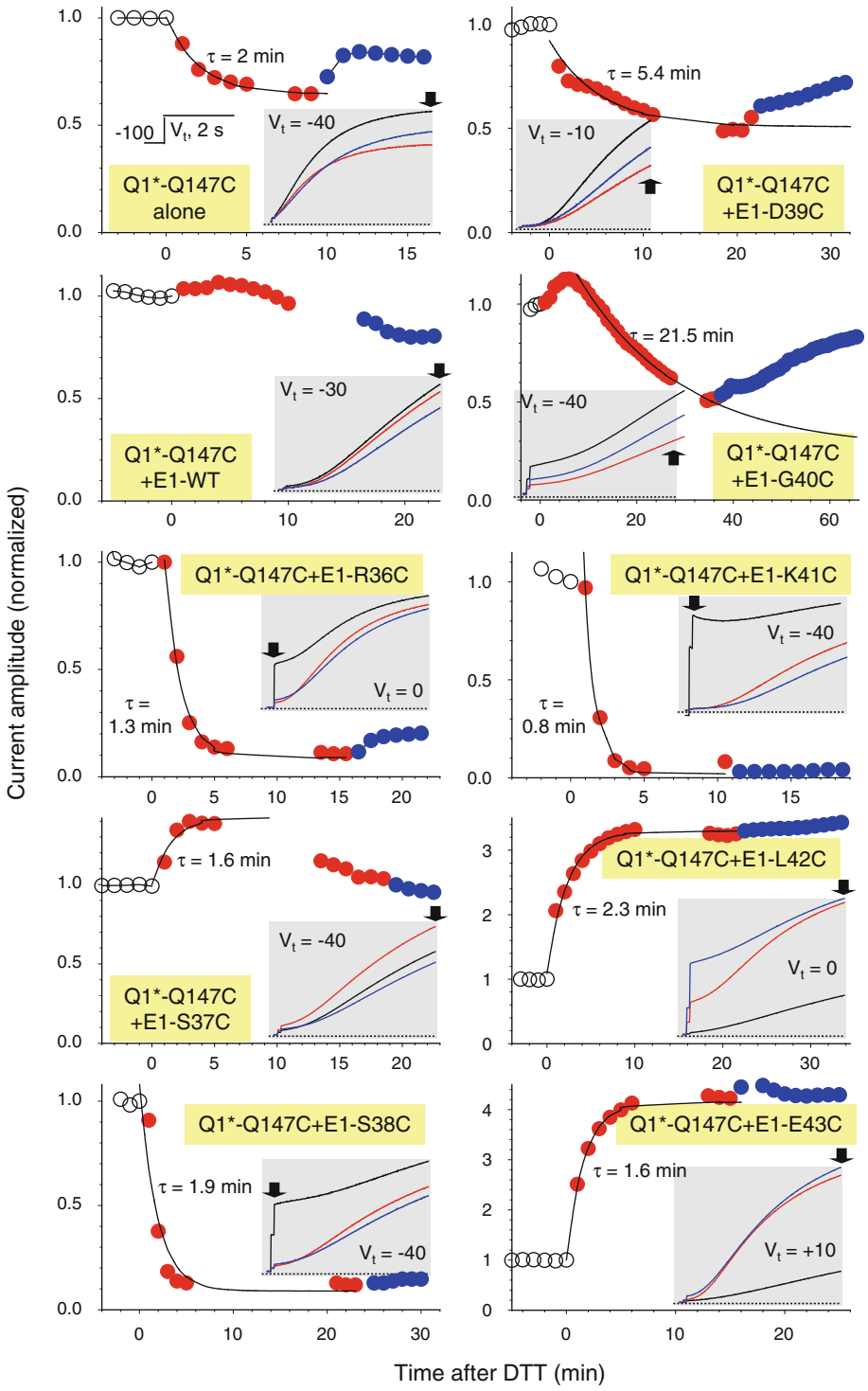

Fig. 6 Representative time courses of changes in the current amplitude of Q1*-Q147C expressed alone or coexpressed with E1 variants before, during, and after DTT (10 mM) exposure, and representative original current traces. In each panel, the channel type is highlighted by *yellow shading,* and the main graph shows time course of changes in current amplitude before (*open black circles*), during (*solid red circles*) and after (*solid blue circles*) DTT exposure. Selected current traces from the same experiment are superimposed in the *inset*, color-coded *black*, *red*, and *blue* for before, during, and after DTT exposure, and highlighted by *gray shading*. The voltage clamp (constant V_t) protocol is diagrammed in the *inset* of the panel for Q1*-Q147C alone: from V_h −100 mV, 2-s depolarizing test pulses to V_t are applied once per minute. The V_t value is noted in each panel, adjacent to the current traces in the *inset*. The time points when current amplitudes are measured are denoted by *solid black arrows:* time-dependent current measured at the end of test pulses (Q1*-Q147C expressed alone, or with E1-WT, S37C, D39C, G40C, L42C or E43C), time-independent (constitutively active) current measured at the beginning of test pulses (Q1*-Q147C coexpressed with E1-R36C, S38C, and K41C). The time course of changes in the current amplitude upon DTT exposure is fit with a single exponential function and is shown as a *smooth black curve* superimposed on the *red solid* data points, with the value of time constant (τ) noted. The gap in *red circle* data points reflects the duration when the voltage dependence of channel activation in the presence of DTT is measured

or no reversal of these dramatic DTT effects (Fig. 8). When expressed in COS-7 cells, the Q1*-T144C/E1-WT pair manifests a prominent constitutive current component, that is abolished by DTT irreversibly (Supplementary Fig. S1B). These observations suggest that in both oocytes and COS-7 cells, Q1*-T144C may be disulfide bonded with Cys on native proteins of the expression systems, and the disulfide bonds stabilize the channels in the activated state. Accordingly, we expect to detect band or bands above the Q1 monomer band in nonreducing Q1 immunoblots of whole cell lysates prepared from Q1*-T144C-expressing oocytes and COS-7 cells. Supplementary Figure S1C shows that no such band can be detected up to 250 kDa. Therefore, the mechanism for the strong DTT

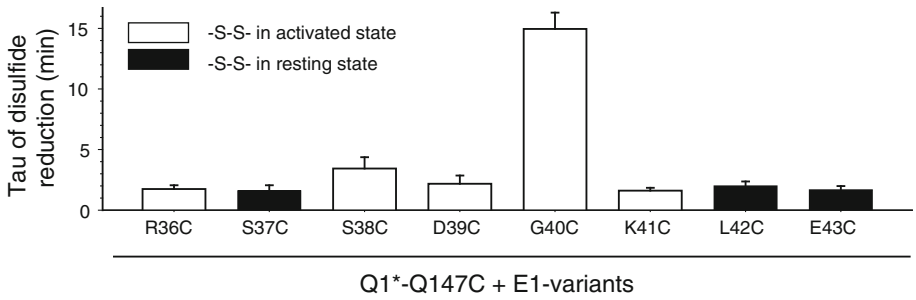

Fig. 7 Time constants of disulfide bond reduction by 10 mM DTT, based on single-exponential fit to the time course of changes in the current amplitude upon DTT exposure as shown in Fig. 6. *Open* and *solid histogram bars* denote disulfide formation in activated and resting states, respectively

effects on Q1*-T144C expressed alone or paired with E1-WT is not clear.

With the above caveat, we proceed to test the effects of DTT on Q1*-T144C paired with Cys-substituted E1 variants. Figure 8 illustrates representative time courses of development of DTT effects on these Q1*-T144C/E1 pairs, with currents monitored at pre-DTT $V_{0.5}$ values. Other than Q1*-T144C/E1-G40C, all the other Q1*-T144C/Cys-substituted E1 pairs manifest a prominent transient increase in the current amplitudes upon DTT exposure. In all cases, this is followed by a gradual decline in the current amplitude in the continuous presence of DTT. Although the latter current declining phase is similar to that seen with Q1*-T144C/E1-WT, the initial transient increase in current likely reflects the consequence of reducing disulfide bonds between Q1* 144C and Cys engineered into the extracellular E1 loop.

What is the mechanism for this transient increase in the current amplitudes? One possible scenario is that disulfide bonds have been formed between the engineered Cys side chains in the resting state. Disulfide reduction by DTT favors channel activation, causing a negative shift in the activation curves and an increase in the current amplitudes monitored at pre-DTT $V_{0.5}$ values. We can detect such a negative $V_{0.5}$ shift after a relatively short DTT exposure (Supplementary Fig. S2C). A more reliable test is to compare the pre-DTT $V_{0.5}$ values among the Q1*-T144C/Cys-substituted E1 pairs and the degrees of transient increase in the current amplitude upon DTT exposure. According to the above scenario, we predict that a more positive pre-DTT $V_{0.5}$ value should be coupled with a more prominent transient increase in the current amplitude upon DTT exposure. Data presented in Fig. 9 confirm this prediction. Given a 4:2 (Q1:E1) stoichiometry in the channel complex (Chen et al. 2003a; Morin and Kobertz 2008), the two Cys side chains at Q1 position 144 that are not disulfide bonded with Cys on E1 are still capable of forming disulfide bonds with oocyte native protein or proteins. These are likely more stable disulfide bonds that can be reduced by DTT only slowly, causing a gradual decline in the current amplitude (Fig. 8) as a result of a positive shift in the voltage dependence of activation.

The COS-7 experiments show that Q1*-T144C and E1-G40C can form a strong disulfide bond (Figs. 3, 4). Exposing oocytes expressing Q1*-T144C/E1-G40C to DTT induces a gradual decline in the current amplitude along with a prominent positive shift in the $V_{0.5}$ value. The degree of DTT-induced positive $V_{0.5}$ shift is significantly higher for Q1*-T144C/E1-G40C (45.3 ± 7.8 mV, $n = 4$) than for Q1*-T144C/E1-WT (19.0 ± 2.7 mV, $n = 12$, $P < 0.001$). With shorter DTT exposure, the decline in the current amplitude develops faster and the positive $V_{0.5}$ shift is more prominent when Q1*-T144C is paired with E1-G40C than with E1-WT (Supplementary Fig. S2; cf. A and B). We propose that a disulfide bond is formed between Q1*-T144C and E1-G40C in the activated state, whose effect on channel gating is additive to that of disulfide bonding between Q1*-T144C and native oocyte proteins, which also stabilizes the channel in the activated state.

State-dependence of Cd-bridge Formation Between Q1*-T144C and Cys Side Chains at E1 Positions 40 and 41

A stringent test for the state-dependence of proximity between two thiol side chains is Cd-bridge formation. Two thiol side chains apart from each other in <5 Å can coordinate a tight Cd-bridge, which cannot be broken by simply removing ambient Cd ions (Castagnetto et al. 2002). Our protocols are diagrammed on top of Fig. 10. All oocytes have been pretreated with 10 mM DTT for 30 min at room temperature (see time courses of DTT effects in Fig. 8) to ensure that all relevant disulfide bonds have been reduced before voltage clamping. We apply a low concentration of Cd ions (100 μM) to Q1*-T144C coexpressed with E1 variants when the channels are held in the resting state (holding voltage −100 mV), or in the activated state (cycling from −100 mV to +90 mV for 2 s and then −20 mV for 2 s, once every 5 s, channels kept in the activated state >98% of the time), The Cd exposure time is 5–8 min. We then thoroughly remove Cd ions by 5–10 min superfusion with Cd-free solution (flow rate 5–6 ml/min). We evaluate the irreversible effects of Cd on the current amplitude and gating kinetics by constructing tail I–V

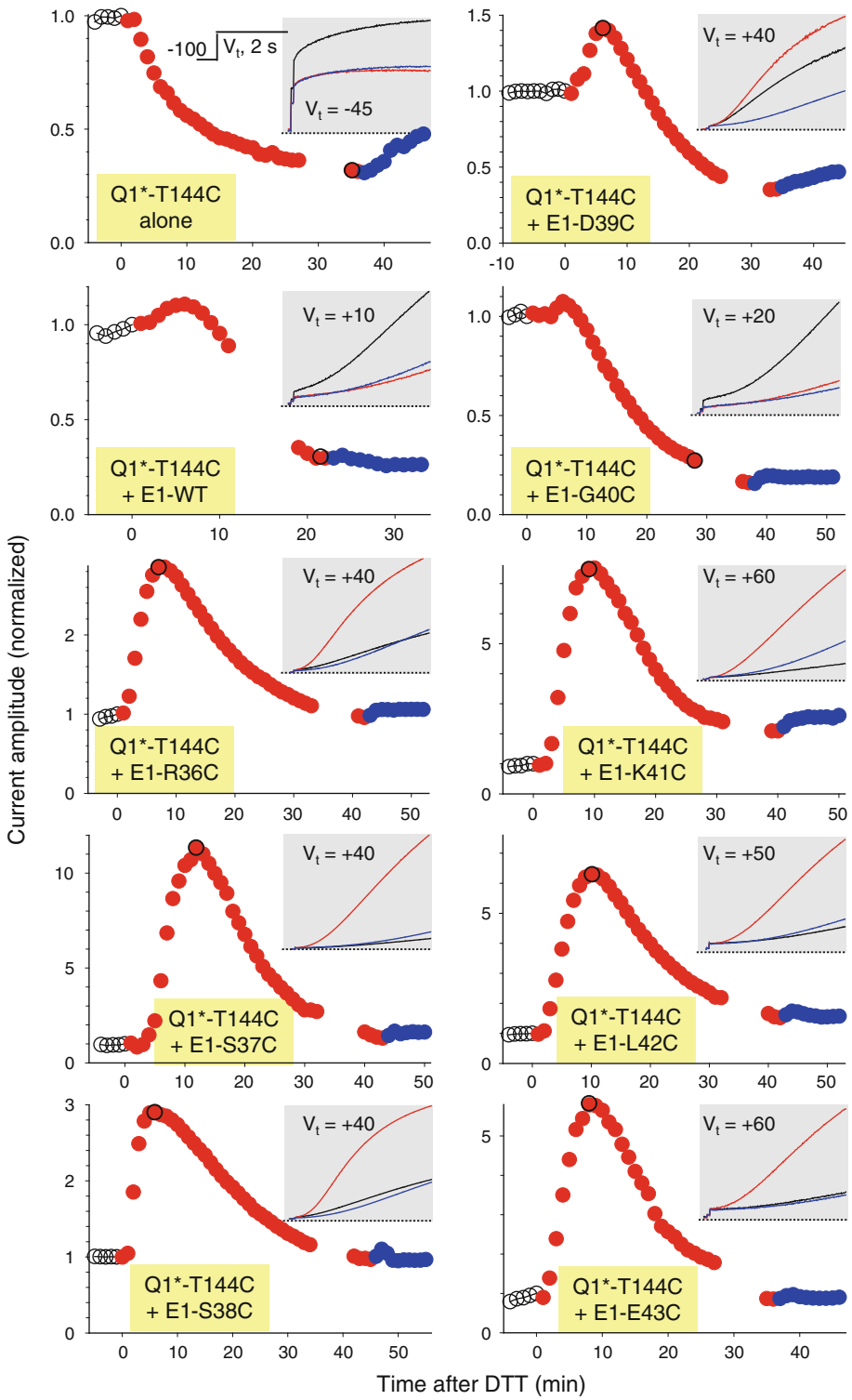

Fig. 8 Representative time courses of changes in current amplitude of Q1*-T144C expressed alone or coexpressed with E1 variants before, during, and after exposure to DTT (10 mM). The format of this figure is similar to that of Fig. 6. For each panel, the channel type is highlighted by *yellow shading*. The main graph depicts the time course of changes in current amplitude. Selected current traces from the same experiment are superimposed in the *inset*, and color coded for before (*black*), during (*red*), and after (*blue*) DTT exposure. The time point when the red current trace (in DTT) is shown is denoted by a *black rim* around the *red data* point in the main graph. The test voltage (V_t) is noted adjacent to the current traces. All the current amplitudes are measured at the end of the 2-s test pulses

relations that cover a wide voltage range (−90 to +140 mV, Fig. 10, upper row). Since our DTT experiments suggest that Q1*-T144C can form disulfides with unidentified proteins in oocytes (Fig. 8), we first test the effects of Cd on Q1*-T144C/E1-WT (Fig. 10a). The protocols themselves without Cd exposure do not affect the current amplitude or gating kinetics. Exposing Q1*-T144C/E1-WT to Cd in either the resting or the activated state causes an increase in the current amplitude and a negative shift in $V_{0.5}$ of activation. These are exactly the opposite of the DTT effects (Fig. 8), and support the notion that disulfide or Cd-bridge formation between Q1*-T144C

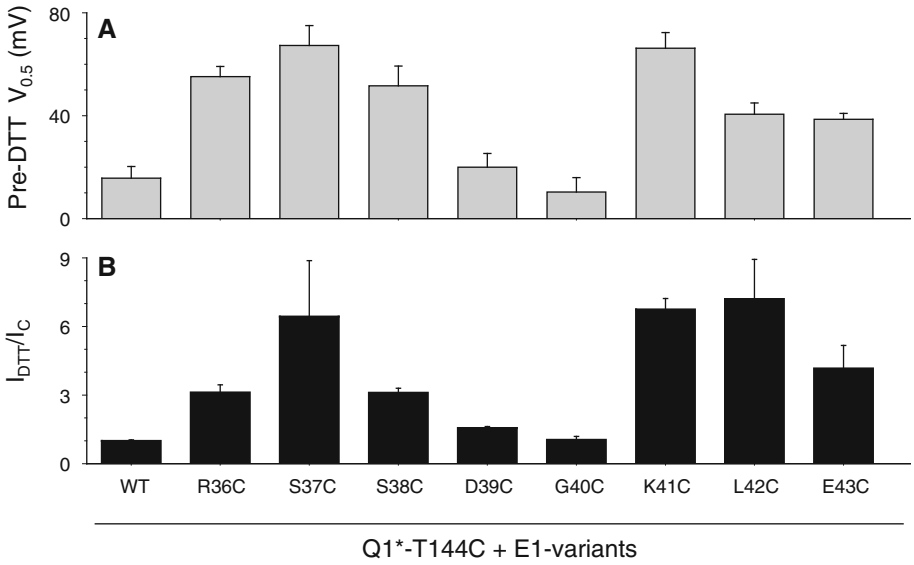

Fig. 9 Correlation between $V_{0.5}$ values for Q1*-T144C/Cys-substituted E1 pairs before DTT exposure (**a**), and the degree of increase in current amplitude when these Q1*-T144C/E1 pairs are exposed to DTT (**b**). $V_{0.5}$ values are estimated as described for Fig. 5. In **b**, data are from experiments similar to those shown in Fig. 8. Current amplitude is measured 8–10 min after the beginning of DTT exposure and normalized by the control current amplitude (I_{DTT}/I_C)

and unidentified proteins in oocytes enhances the current amplitude and stabilizes the activated state. Although Q1*-T144C can form Cd-bridges with native protein partners in both resting and activated states, the partners likely differ. This is based on the observation that a small constitutive current component of Q1*-T144C/E1-WT is greatly enhanced by Cd exposure in the activated state, but suppressed by Cd exposure in the resting state (inset, Fig. 10a, left).

Exposing Q1*-T144C/E1-G40C to Cd in the resting state has little effects on either current amplitude or gating kinetics. However Cd exposure in the activated state greatly increases the constitutive current component and causes a prominent negative shift in the $V_{0.5}$ of activation (Fig. 10b). These observations fully support our proposal that Q1*-T144C comes close to E1-G40C in the activated state to allow disulfide or Cd-bridge formation, which in turn stabilizes the channel in the activated state.

Exposing Q1*-T144C/E1-K41C to Cd in the resting state markedly suppresses the constitutive current component and causes a prominent positive shift in $V_{0.5}$ of activation (Fig. 10c). On the other hand, Cd exposure in the activated state has little effects on Q1*-T144C/E1-K41C. These observation support our proposal that Q1*-T144C and E1-K41C come close to each other in the resting state to allow disulfide or Cd-bridge formation, which stabilizes the channel in the resting state.

Cross Linking Q1*-T144C with Cys Side Chains on E1

In COS-7 experiments, we cannot detect significant disulfide bonds between Q1*-T144C and Cys engineered into E1 positions 36–39, 42 or 43 (Figs. 3, 4). However, in oocyte experiments, exposing these Q1*-T144C/E1 pairs to DTT induces a prominent transient increase in the current amplitudes, which is interpreted as the result of reducing disulfide bonds formed between these engineered Cys side chains in the resting states. To check whether Q1*-T144C can form disulfide bonds with Cys at these E1 positions in oocytes, we probe membrane fractions prepared from oocytes expressing Q1*-T144C/E1 pairs. If oocytes are pretreated with NEM before membrane solubilization, we cannot detect disulfide formation in the Q1*-T144C/Cys-substituted E1 pairs (Supplementary Fig. S3, top panel). However, it we omit the NEM pretreatment, we can detect faint disulfide formation between Q1*-T144C and E1-R36C–K41C (Supplementary Fig. S3, middle vs. bottom panels). These observations suggest that Q1*-T144C can form weak and transient disulfide bonds with Cys at these E1 positions in oocytes. However, the linkage is so unstable that it can be prevented by NEM treatment.

An alternative method to probe the proximity between thiol side chains is to use bifunctional thiol-reactive cross-linkers. We test whether we can cross link Q1*-T144C with Cys at E1 positions 37, 39. 41 and 42 using methanethiosulfonate cross-linkers (MxM, where x refers to the number of spacer arm carbons). We use M3M, M5M and M6M, with spacer arm lengths between 6.6 and 11.2 Å (Fig. 11). COS-7 cells coexpressing Q1*-T144C with E1-WT (negative control) or Cys-substituted E1 variants are DTT-treated, rinsed, and exposed to 2 mM MxM for 15 min at 4°C. The reaction is stopped by adding 10 mM NEM. The cells are lysed and whole cell lysates are analyzed by SDS-PAGE/immunoblotting under nonreducing conditions. Treating each of these

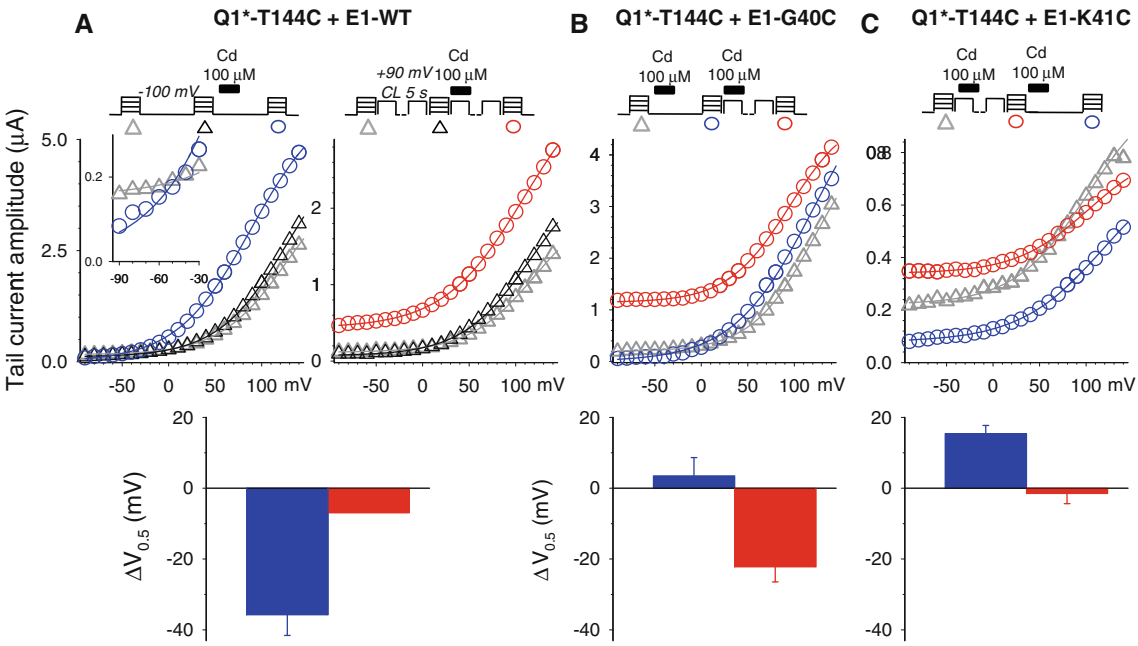

Fig. 10 Effects of Cd (100 µM) on Q1*-T144C coexpressed with E1-WT (**a**), E1-G40C (**b**), or E1-K41C (**c**), and deduction of the state-dependence of Cd-bridge formation between the latter 2 double Cys-substituted Q1*-T144C/E1 pairs. In each panel, the *upper row* shows tail I–V relationships obtained under conditions depicted by the diagram on *top*: (1) first control tail I–V (*gray open triangles*) before any intervention, (2) second control tail I–V (*black open triangles*) after the oocyte membrane has been held at −100 mV for 12 min (**a**, *left*), or after the oocyte membrane has been pulsed from −100 mV to +90 mV for 2 s, and then −20 mV for 2 s, applied once every 5 s (**a**, *right*), (3) tail I–V after exposure to Cd for 5 min while the membrane is held at −100 mV (*blue open circles,* Cd exposure in the resting state), and (4) tail I–V after exposure to Cd for 5 min while the membrane is pulsing through −90 mV/− 20 mV as described above (*red open circles,* Cd exposure in the activated state). Note that Cd is washed out for 5–10 min before (3) or (4) is recorded. The tail I–V is fit with a Boltzmann function similar to the one described for Table 1, except that a constitutive component (I_{SS}) is included: $I_{tail} = I_{max}/[1 + \exp((V_{0.5} - V_t)/k)] + I_{SS}$. Cd-induced shift in the $V_{0.5}$ value is summarized in the lower row, with *blue histogram bars* representing Cd exposure in the resting state, and *red bars* for Cd exposure in the activated state. *Inset* in **a**, *left* amplified I–V relationships to illustrate that Cd exposure in the resting state suppresses the small constitutive current component of Q1*-T144C/E1-WT

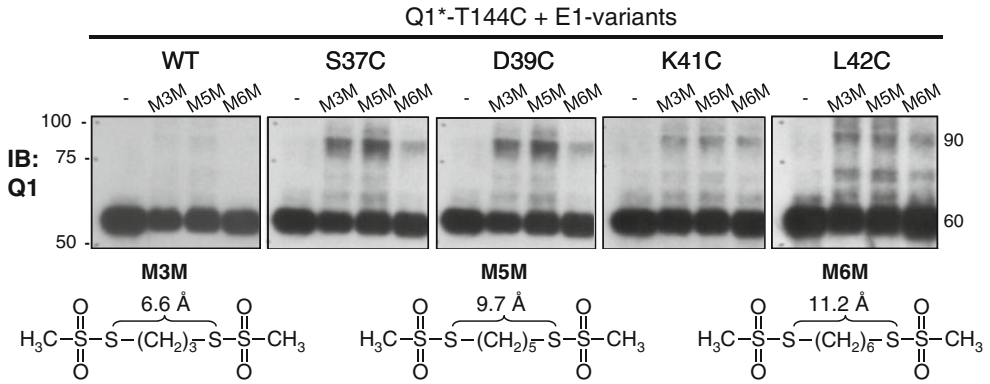

Fig. 11 Using bifunctional thiol-reactive methanethiosulfonate cross-linkers of different spacer arm lengths to probe the proximity between 144C on Q1* and Cys on E1 positions 37, 39, 41, and 42. Q1*-T144C/E1-WT serves as negative control. COS-7 cells expressing the specified Q1*-T144C and E1 variants are incubated in 2 mM cross-linker for 15 min at 4°C (M3M, M5M, M6M, structures and the spacer arm lengths shown). Whole-cell lysates are analyzed by nonreducing immunoblotting targeting Q1*. The major cross-linked Q1*/E1 band is 90 kDa, while the Q1* monomer is 60 kDa. Spacer arm lengths are calculated based on bond lengths of 1.52 Å for C–C and 1.82 Å for C–S

Q1*-T144C/Cys-substituted E1 pairs with cross-linkers produces a distinct 90 kDa band. This band is not seen in samples without reaction with the cross-linkers, or in Q1*-T144C/E1-WT after treatment with the cross-linkers (Fig. 11), confirming that it represents cross-linked Q1*-T144C/E1 heterodimers.

Requirements for Side Chain Properties at Q1 Positions 143 and 146 for Proper Q1 and I_{Ks} Channel Function

In COS-7 immunoblot experiments, Q1*-S143C and Q1*-E146C migrate as doublet bands below the 60 kDa Q1 monomer bands seen in the other Q1* variants (Fig. 12a, left). This smaller band size of Q1*-S143C and Q1*-E146C may reflect immature, poorly glycosylated proteins that fail to reach the cell surface (Supplementary Fig. S4). Patch clamp experiments show that COS-7 cells transfected with Q1*-S143C cDNA express little or no time-dependent currents, while the same batch of cells transfected with an

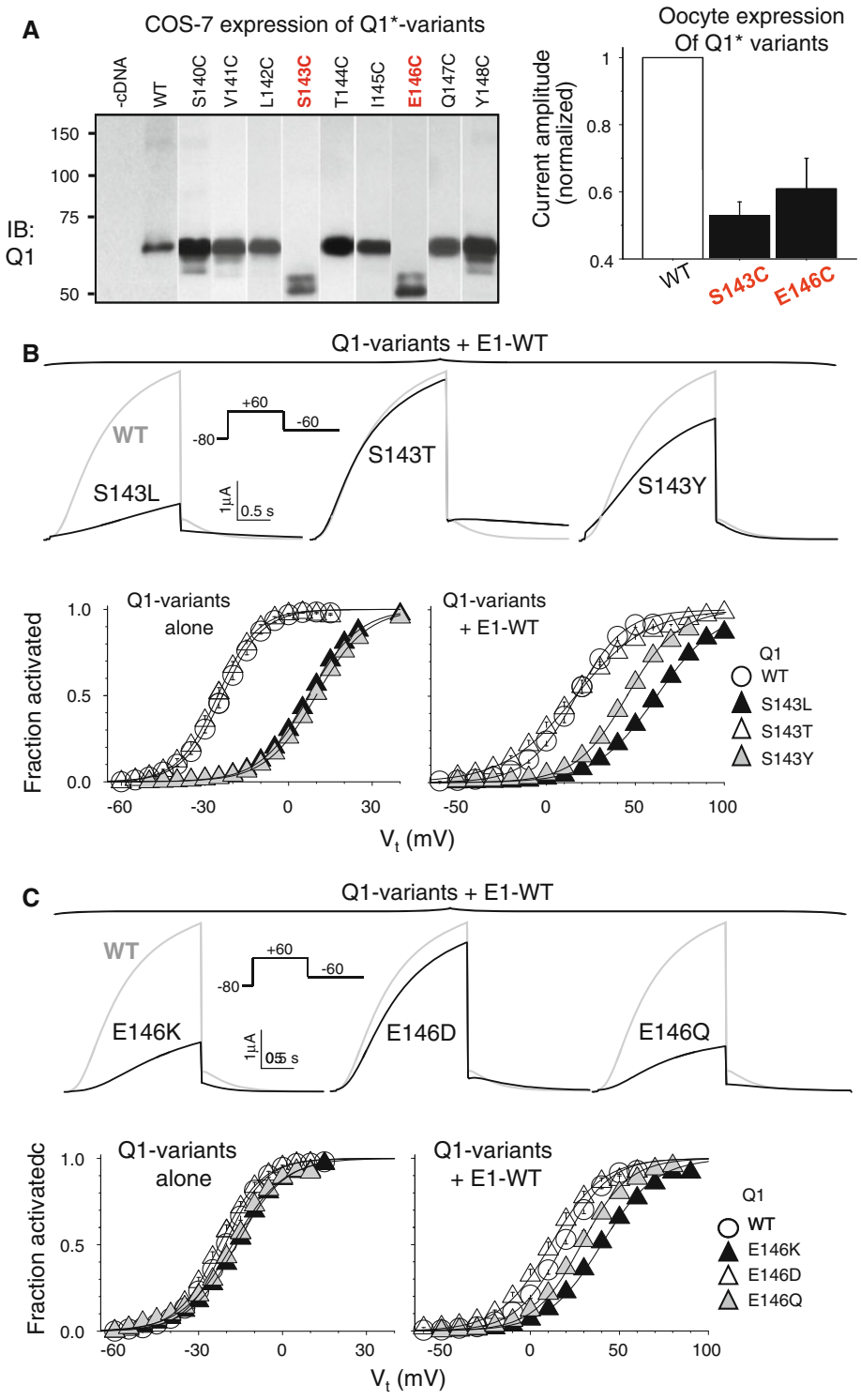

Fig. 12 Cys substitution at Q1 positions 143 and 146 impairs Q1 channel function, while more conservative mutations at these two positions better preserve channel function. **a** *Left* Different migration patterns of Q1*-S143C and Q1*-E146C in SDS-PAGE, relative to those of Q1*-WT and other Cys-substituted Q1* mutants expressed in COS-7 cells. *Right* Reduced current amplitudes of Q1*- S143C and Q1*-E146C relative to that of Q1*-WT expressed in oocytes. **b** Replacing serine at Q1 position 143 with threonine preserves the channel function while replacement with leucine or tyrosine causes different degrees of impairment. *Top* Comparison of current traces of Q1-S143L, Q1-S143T, and Q1-S143Y (*black traces*) with that of Q1-WT (*gray trace*) coexpressed with E1-WT in oocytes. The voltage clamp protocol is diagrammed in the *inset*. *Bottom* Voltage dependence of activation of Q1-WT, Q1-S143L, Q1-S143T, and Q1-S143Y expressed alone (*left*) or coexpressed with E1-WT (*right*). The same set of symbols (*inset of right panel*) is used for both panels. **c** Effects of replacing glutamate at Q1 position 146 with lysine, aspartate, and glutamine (E146K, E146D, and E146Q) on Q1 channel function and Q1/E1 interactions. The format is the same as that in **b**. In **b** and **c**, the Q1-WT has all the native Cys residues, and the mutations are made in this parent Q1-WT background

equivalent amount of Q1*-WT cDNA express robust currents (data not shown). In oocytes injected with equivalent amounts of cRNA, Q1*-S143C and Q1*-E146C produce much less currents than Q1*-WT (Fig. 12a, right). Therefore, positions 143 and 146 are high-impact positions that cannot tolerate Cys substitution. These two positions may intimately interact with other Q1 domains so that they have more stringent requirements for side chain properties.

S143L and E146K are two LQT1-related mutations (Liu et al. 2006; Napolitano et al. 2005). How they impact the I_{Ks} channel function is not clear. To address this question and to probe the requirement for side chain properties at these two high-impact positions, we make a series of mutations at positions 143 (S143L, S143T and S143Y) and 146 (E146K, E146D and E146Q). These mutations are made in the parent Q1-WT background (containing all native Cys residues), and their impact on the Q1 and Q1/E1 channel function are examined in oocyte experiments. The lower temperature used in oocyte incubation (16°C) allows mildly misfolded proteins to traffic to the cell surface, making it possible to examine their channel biophysical properties. Data are summarized in Fig. 12b, c and Table 3.

Replacing S143 with threonine (preserving the hydroxyl group and modestly increasing the side chain volume from 89.0 to 116.1 $Å^3$) does not perturb the Q1 channel function, alone or with E1-WT. Replacing S143 with leucine (removing the hydroxyl group and markedly increasing the side chain volume to 166.7 $Å^3$) right shifts the activation curve, more so when coexpressed with E1-WT (by 41.2 ± 2.4 mV) than alone (by 30.6 ± 1.1 mV). Replacing S143 with tyrosine (preserving the hydroxyl group but markedly increasing the side chain volume to 193.6 $Å^3$) right shifts the activation curve expressed alone (by 30.5 ± 1.5 mV) or coexpressed with E1-WT (by 27.0 ± 2.7 mV). These data indicate that position 143 requires a small side chain with a hydroxyl group to ensure proper Q1 function. The S143L mutation shifts the voltage dependence of I_{Ks} activation to a much more positive range than the WT channel, thus producing the loss-of-function phenotype.

Replacing E146 with aspartate (preserving the negative charge and modestly reducing the side chain volume from 138.4 to 111.1 $Å^3$) does not perturb the Q1 channel function expressed alone or coexpressed with E1-WT. Replacing E146 with lysine (reversing the charge and increasing the side chain volume to 168.6 $Å^3$) has little effect on the Q1 channel function when expressed alone ($V_{0.5}$ right shifted by only 4.1 ± 1.2 mV), but causes a prominent right shift in the activation curve when coexpressed with E1-WT (by 21.6 ± 2.4 mV). Replacing E146 with glutamine (neutralizing the charge but preserving the side chain volume at 143.9 $Å^3$) creates a phenotype similar to that of E146K. Thus, the negative charge at position 146 is critical. The E146K mutation creates a loss-of-function phenotype by shifting the voltage dependence of I_{Ks} activation in the positive direction.

Table 3 Effects of S143 and E146 mutations on the KCNQ1 channel function when expressed alone or coexpressed with KCNE1-WT[a]

Q1 variant	E1	$V_{0.5}$ (mV)	z_g	ΔG_o (kcal/mol)	*n*
WT	–	−20.6 ± 0.8	3.55 ± 0.08	−1.76 ± 0.08	25
WT	WT	18.3 ± 1.4	1.96 ± 0.05	0.86 ± 0.07	21
S143L	–	10.0 ± 0.7	2.87 ± 0.07	0.68 ± 0.05	23
S143L	WT	59.5 ± 1.9	1.52 ± 0.04	2.15 ± 0.05	21
S143T	–	−25.4 ± 0.9	3.58 ± 0.10	−2.19 ± 0.12	12
S143T	WT	16.3 ± 3.0	1.27 ± 0.05	0.49 ± 0.09	9
S143Y	–	9.9 ± 1.3	2.83 ± 0.12	0.64 ± 0.06	10
S143Y	WT	45.3 ± 2.3	1.76 ± 0.07	1.90 ± 0.11	9
E146K	–	−16.5 ± 0.9	2.99 ± 0.12	−1.21 ± 0.10	16
E146K	WT	39.9 ± 1.9	1.70 ± 0.06	1.60 ± 0.07	23
E146D	–	−22.5 ± 1.1	3.33 ± 0.09	−1.82 ± 0.13	10
D146D	WT	11.4 ± 2.4	1.74 ± 0.05	0.47 ± 0.10	10
E146Q	–	−17.9 ± 0.7	2.84 ± 0.13	−1.23 ± 0.08	13
E146Q	WT	28.6 ± 3.3	1.90 ± 0.04	1.29 ± 0.14	10

[a] All mutations are made in the parent Q1-WT construct that contains all native Cys side chains. Oocytes are injected with cRNAs for Q1 variant alone or with E1-WT (10 and 3 ng, Q1:E1 cRNA molar ratio 1:1). Voltage clamp protocol and data analysis are the same as those described for Table 1

Discussion

Our major findings are summarized in Fig. 13a. The pattern of contacts between Q1* and E1 in the region of interest is based on the detection of disulfide bonded Q1*/E1 heterodimers in nonreducing immunoblots from COS-7 cells (Fig. 4). The degree of disulfide bond formation is quantified by the ratio of band intensities between disulfide bonded Q1*/E1 heterodimer (80 kDa) and the Q1* monomer (60 kDa). Disulfide-forming Q1*/E1 pairs are linked by arrows with line color and thickness reflecting the 80:60 band ratio (color scheme shown on the bottom). The assignment of gating states (resting or activated) in which Q1*/E1 contacts occur is based on voltage clamp data from oocytes (Figs. 5–10) (Xu et al. 2008).

Molecular Motions in the Extracellular Juxtamembranous Region of I_{Ks} During Gating Transitions and Implications in I_{Ks} Channelopathy

Figure 13b depicts the proposed orientation of Q1 positions examined here relative to E1 and the other transmembrane helices of the Q1 channel. We propose that positions 144,

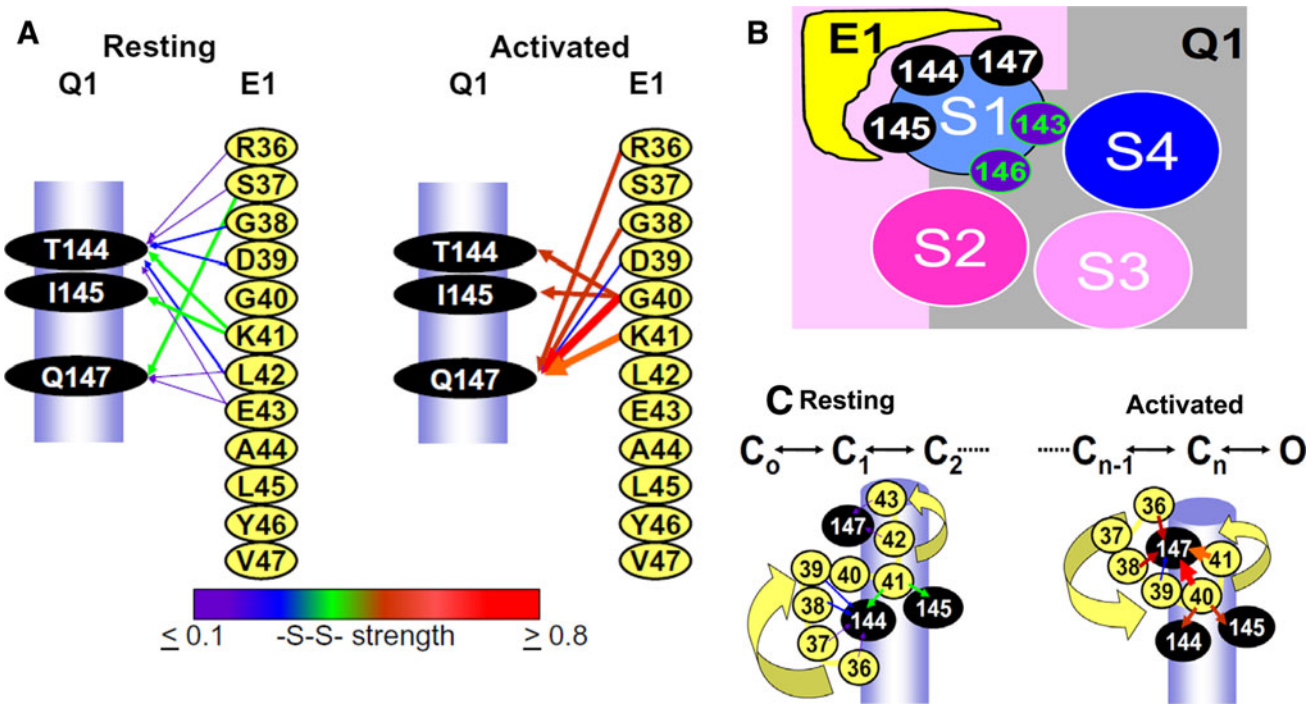

Fig. 13 Implication of our data for conformational changes in the Q1/E1 channel complex during gating transitions. **a** Degree and state dependence of disulfide bond formation between Q1* positions 144, 145, and 147 and E1 positions 36–43. The thickness and color of *arrows* linking E1 to Q1 positions are based on the ratio of 80:60 kDa band intensities (Fig. 4). The color scheme is shown below. **b** Cartoon of proposed relationship between Q1 positions examined here and the E1 extracellular juxtamembranous loop, as well as the other transmembrane helices in the voltage-sensing domain of the same Q1 subunit. **c** Putative molecular motions of E1 relative to Q1 in different gating states

145 and 147 are facing the cleft between Q1 voltage-sensing domains. They can interact with the extracellular juxtamembranous E1 loop (denoted by the yellow shading) when E1 occupies this space. The cartoon in Fig. 13c depicts one possibility of what may be happening in the extracellular juxtamembranous region of the I_{Ks} channel during gating transitions. At negative membrane voltages when the channels are making transitions through resting states, there are molecular motions in this region of the I_{Ks} channel so that E1 positions 36 to 43 pass by Q1 positions 144, 145 and147 in a parallel fashion. The consecutive contacts between these E1 positions and Q1 position 144 allow disulfide bond formation when they are occupied by engineered Cys residues. Furthermore, E1 position 41 comes close to Q1 position 145, and E1 positions 42 and 43 reach Q1 position 147, to allow disulfide bond formation. At depolarized voltages when the channels are making transitions among activated states, E1 position 40 becomes very active and can come close to Q1 positions 144, 145 and 147 to allow disulfide bond formation. Furthermore, the surrounding E1 positions (36, 38, 39 and 41) pass by or wrap around Q1 position 147 to allow disulfide bond formation.

We propose that the extracellular juxtamembranous E1 loop and the S1–S2 linker of the Q1 channel make multiple and dynamic contacts with each other during the I_{Ks} channel gating transitions. This scenario provides insights into how mutations in this region can impair the I_{Ks} channel function, i.e. I_{Ks} channelopathy. An LQT1-related mutation at Q1 position 147, Q147R, behaves like the WT channel when expressed alone. However, when coexpressed with E1-WT, Q147R manifests a loss-of-function phenotype (reduced I_{Ks} current amplitude). Our data suggest that Q1 position 147 comes close to E1 positions 36 and 41 in the activated states (Fig. 13a). It is conceivable that in I_{Ks} channels bearing the Q147R mutation, the contacts between Q1 position 147 (occupied by a positively charged arginine) with E1 position 36 (arginine) and 41 (lysine) are hindered by electrostatic repulsion. This may destabilize the activated state of the I_{Ks} channel, causing a loss-of-function phenotype.

We place positions 143 and 146 facing the other parts of the Q1 channel, assumed to be the other transmembrane helices in the voltage-sensing domain of the same Q1 subunit (based on the Kv1.2 crystal structure, Fig. 1a). This orientation is consistent with the observations that Cys substitution at these 2 positions impairs the Q1 channel function. We propose that position 143 requires a small side chain with a hydroxyl group, as if it needs to form hydrogen bonds with other Q1 residues to stabilize the

folding and sustain proper I_{Ks} gating kinetics. Position 146 requires a negatively charged side chain, as if it needs to form salt bridges with oppositely charged residues on other Q1 domains to stabilize the folding and support proper I_{Ks} gating kinetics. These scenarios can explain the loss-of-function phenotypes of LQT1-related S143L and E146K.

Technical Consideration: COS-7 Cells vs Oocytes

There are differences between COS-7 experiments and oocyte experiments. Several Q1*/E1 pairs that show only weak disulfide bond formation in COS-7 experiments (ratio of 80:60 kDa band intensities <0.1) manifest prominent and distinct responses to DTT in oocyte experiments. These Q1*/E1 pairs are linked by thin blue arrows in Fig. 13a. The most striking contrast is seen in Q1*-T144C/E1-S37C. This Q1*/E1 pair shows little or no disulfide bond formation in COS-7 experiments (Figs. 3a, 4). Yet in oocyte experiments, DTT exposure produces a surge in the current amplitude, reaching a level 10 times of control (Fig. 8). To reconcile this difference, we show that these two thiol side chains in the COS-7 cell membrane can come close to each other to be cross-linked by bifunctional methanethiosulfonate linkers with spacer arms 6.6–11.2 Å in length. Furthermore, in oocytes we can detect a very faint Q1*-T144C/E1-S37C heterodimer band if the oocytes are not treated with NEM before membrane solubilization. It is possible that in COS-7 cells cultured under the static conditions, there is limited peptide backbone flexibility in the Q1*/E1 channel complex. Thus, there is a low frequency of Cys side chain encounters, and little or no disulfide bond formation. On the other hand, in oocyte experiments, the cycling of membrane voltage triggers gating transitions in the Q1*/E1 channel complex, allowing a high flexibility of the peptide backbones and a high frequency of Cys side chain encounters. These encounters promote weak and transient disulfide bond formation, whose functional consequences can be detected by DTT treatment in voltage clamp experiments.

Acknowledgments This study was supported by RO1 HL67840 from National Heart, Lung and Blood Institute, and R21 AT0044601 from National Center for Complementary and Alternative Medicine, of National Institutes of Health (to GNT).

References

Bendahhou S, Marionneau C, Haurogne K, Larroque MM, Derand R, Szuts V, Escande D, Demolombe S, Barhanin J (2005) In vitro molecular interactions and distribution of KCNE family with KCNQ1 in the human heart. Cardiovasc Res 67:529–538

Campos FV, Chanda B, Roux B, Bezanilla F (2007) Two atomic constraints unambiguously position the S4 segment relative to S1 and S2 segments in the closed state of Shaker K channel. Proc Natl Acad Sci USA 104:7904–7909

Careaga CL, Falke JJ (1992) Thermal motions of surface α-helices in the D-galactose chemosensory receptor. Detection by disulfide trapping. J Mol Biol 226:1219–1235

Castagnetto JM, Hennessy SW, Roberts VA, Getzoff ED, Tainer JA, Pique ME (2002) MDB: the mtalloprotein database and browser at the Scripps Research Institute. Nucleic Acids Res 30:379–382

Chen H, Kim LA, Rajan S, Xu S, Goldstein SAN (2003a) Charybdotoxin binding in the I_{Ks} pore demonstrates two minK subunits in each channel complex. Neuron 40:15–23

Chen YH, Xu SJ, Bendahhou S, Wang XL, Wang Y, Xu WY, Jin HW, Sun H, Su XY, Zhuang QN, Yang YQ, Li YB, Liu Y, Xu HJ, Li XF, Ma N, Mou CP, Chen Z, Barhanin J, Huang W (2003b) KCNQ1 gain-of-function mutation in familial atrial fibrillation. Science 299:251–254

Chung DY, Chan PJ, Bankston JR, Yang L, Liu G, Marx SO, Karlin A, Kass RS (2009) Location of KCNE1 relative to KCNQ1 in the I_{Ks} potassium channel by disulfide cross-linking of substituted cysteines. Proc Natl Acad Sci USA 106:743–748

Cuello LG, Cortes DM, Perozo E (2004) Molecular architecture of the KvAP voltage-dependent K^+ channel in a lipid bilayer. Science 306:491–495

Fan JS, Jiang M, Dun W, McDonald TV, Tseng GN (1999) Effects of outer mouth mutations on *hERG* channel function: a comparison with similar mutations in *Shaker*. Biophys J 76:3128–3140

Ghosh S, Nunziato DA, Pitt GS (2006) KCNQ1 assembly and function is blocked by long-QT syndrome mutations that disrupt interaction with calmodulin. Circ Res 98:1048–1054

Grunnet M, Olesen SP, Klaerke DA, Jespersen T (2005) hKCNE4 inhibits the hKCNQ1 potassium current without affecting the activation kinetics. Biochem Biophys Res Commun 328:1146–1153

Haitin Y, Wiener R, Shaham D, Peretz A, Cohen EBT, Shamgar L, Pongs O, Hirsch JA, Attali B (2009) Intracellular domains interactions and gating motions of I_{Ks} potassium channel subunits. EMBO J 28:1994–2005

Hong K, Piper DR, Diaz-Valdecantos A, Brugada J, Oliva A, Burashnikov E, Santos-de-Soto J, Grueso-Montero J, Diaz-Enfante E, Brugada P, Saches F, Sanguinetti MC, Brugada R (2005) De novo KCNQ1 mutation responsible for atrial fibrillation and short QT syndrome in utero. Cardiovasc Res 68:433–440

Jost M, Virag L, Bitay M, Takacs J, Lengyel C, Biliczki P, Nagy Z, Bogats G, Lathrop DA, Papp JG, Varro A (2005) Restricting excessive cardiac action potential and QT prolongation. A vital role for I_{Ks} in human ventricular muscle. Circulation 112:1392–1399

Kang C, Tian C, Sonnichsen FD, Smith JA, Meiler J, George AL Jr, Vanoye CG, Kim HJ, Sanders CR (2008) Structure of KCNE1 and implications for how it modulates the KCNQ1 potassium channel. Biochemistry 47:7999–8006

Kapplinger JD, Tester DJ, Salisbury BA, Carr JL, Harris-Kerr C, Pollevick GD, Wilde AAM, Ackerman MJ (2009) Spectrum and prevalence of mutations from the first 2500 consecutive unrelated patients referred for the FAMILION long QT syndrome genetic test. Heart Rhythm 6:1297–1303

Kurokawa J, Bankston JR, Kaihara A, Chen L, Furukawa T, Kass RS (2009) KCNE variants reveal a critical role of the β subunit carboxyl terminus in PKA-dependent regulation of the I_{Ks} potassium channel. Channels 3:1–9

Liu WL, Hu DY, Li P, Li CL, Qin XG, Li YT, Li L, Li ZM, Dong W, Qi Y, Wang Q (2006) Novel mutations of potassium channel KCNQ1 S143L and KCNH2 Y475C genes in Chinese pedigrees of long QT syndrome. Zhonghua Nei Ke Za Zhi 45:463–466

Liu XS, Zhang M, Jiang M, Wu DM, Tseng GN (2007) Probing the interaction between KCNE2 and KCNQ1 in the transmembrane region. J Memb Biol 216:117–127

Long SB, Campbell EB, MacKinnon R (2005) Crystal structure of a mammalian voltage-dependent *Shaker* family K^+ channel. Science 309:897–903

Lundby A, Raven LS, Svendsen JH, Olesen SP, Schmitt N (2007) KCNQ1 mutation Q147R is associated with atrial fibrillation and prolonged QT-interval. Heart Rhythm 4:1532–1541

Lundquist AL, Manderfield LJ, Vanoye CG, Rogers CS, Donahue BS, Chang PA, Drinkwater DC, Murray KT, George AL Jr (2005) Expression of multiple KCNE genes in human heart may enable variable modulation of I_{Ks}. J Mol Cell Cardiol 38:277–287

Lvov A, Gage SD, Berrios VM, Kobertz WR (2010) Identification of a protein–protein interaction between KCNE1 and the activation gate machinery of KCNQ1. J Gen Physiol 135:607–618

Melman YF, Demenech A, de la Luna S, McDonald TV (2001) Structural determinants of KvLQT1 control by the KCNE1 family of proteins. J Biol Chem 276:6439–6444

Morin TJ, Kobertz WR (2008) Counting membrane-embedded KCNE β-subunits in functioning K^+ channel complexes. Proc Natl Acad Sci USA 105:1478–1482

Nakajo K, Kubo Y (2007) KCNE1 and KCNE3 stabilize and/or slow voltage sensing S4 segment of KCNQ1 channel. J Gen Physiol 130:269–281

Nakajo K, Ulbrich MH, Kubo Y, Isacoff EY (2010) Stoichiometry of the KCNQ1–KCNE1 ion channel complex. Proc Natl Acad Sci USA 107:18862–18867

Napolitano C, Priori SG, Schwartz PJ, Bloise R, Ronchetti E, Nastoli J, Bottelli G, Cerrone M, Leonardi S (2005) Genetic testing in the long QT syndrome. Development and validation of an efficient approach to genotyping in clinical practice. JAMA 294:2975–2980

Panaghie G, Tai KK, Abbott GW (2006) Interaction of KCNE subunits with the KCNQ1 K^+ channel pore. J Physiol 570: 455–467

Radicke S, Dotella D, Graf EM, Banse U, Jost N, Varro A, Tseng GN, Ravens U, Wettwer E (2006) Functional modulation of the transient outward current I_{to} by KCNE β-subunits and regional distribution in human non-failing and failing hearts. Cardiovasc Res 71:695–703

Sanguinetti MC, Curran ME, Zou A, Shen J, Spector PS, Atkinson DL, Keating MT (1996) Coassembly of KvLQT1 and minK (IsK) proteins to form cardiac I_{Ks} potassium channel. Nature 384:80–83

Schreibmayer W, Lester HA, Dascal N (1994) Voltage clamping of *Xenopus laevis* oocytes utilizing agarose-cushion electrodes. Pflugers Arch 426:453–458

Sesti F, Goldstein SAN (1998) Single-channel characteristics of wild-type I_{Ks} channels and channels formed with two minK mutants that cause long QT syndrome. J Gen Physiol 112:651–663

Shamgar L, Ma L, Schmitt N, Haitin Y, Peretz A, Wiener R, Hirsch J, Pongs O, Attali B (2006) Calmodulin is essential for cardiac I_{Ks} channel gating and assembly. Impaired function in long-QT mutations. Circ Res 98:1055–1063

Splawski I, Shen J, Timothy KW, Lehmann MH, Priori SG, Robinson JL, Moss AJ, Schwartz PJ, Towbin JA, Vincent GM, Keating MT (2000) Spectrum of mutations in long-QT syndrome genes *KvLQT1*, *HERG*, *SCN5A*, *KCNE1*, and *KCNE2*. Circulation 102:1178–1185

Tai KK, Goldstein SAN (1998) The conduction pore of a cardiac potassium channel. Nature 391:605–608

Tapper AR, George AL Jr (2001) Location and orientation of minK within the I_{Ks} potassium channel complex. J Biol Chem 276:38249–38254

Tseng-Crank JCL, Tseng GN, Schwartz A, Tanouye MA (1990) Molecular cloning and functional expression of a potassium channel cDNA isolated from a rat cardiac library. FEBS Lett 268:63–68

Wiener R, Haitin Y, Shamgar L, Fernandez-Alonso MC, Martos A, Chomsky-Hecht O, Rivas G, Attali B, Hirsch JA (2008) The KCNQ1 (Kv7.1) COOH terminus, a multitiered scaffold for subunit assembly and protein interaction. J Biol Chem 283:5815–5830

Wu DM, Lai LP, Zhang M, Wang HL, Jiang M, Liu XS, Tseng GN (2006) Characterization of an LQT5-related mutation in KCNE1, Y81C: implications for a role of KCNE1 cytoplasmic domain in I_{Ks} channel function. Heart Rhythm 3:1031–1040

Xu XL, Jiang M, Hsu KL, Zhang M, Tseng GN (2008) KCNQ1 and KCNE1 in the I_{Ks} channel complex make state-dependent contacts in their extracellular domains. J Gen Physiol 131: 589–603

Yang Y, Sigworth FJ (1998) Single-channel properties of I_{Ks} potassium channels. J Gen Physiol 112:665–678

Zareba W, Moss AJ, Sheu G, Kaufman ES, Priori SG, Vincent GM, Towbin JA, Benhorin J, Schwartz PJ, Napolitano C, Hall WJ, Keating MT, Qi M, Robinson JL, Andrews AL (2003) Location of mutation in the KCNQ1 and phenotype presentation of long QT syndrome. J Cardiovasc Electrophysiol 14:1149–1153